J Chem Biol (2013) 6:97–120
DOI 10.1007/s12154-013-0096-3

REVIEW

Fluorescence nanoscopy. Methods and applications

Jose Requejo-Isidro

Received: 6 March 2013 / Accepted: 5 May 2013 / Published online: 4 June 2013

Abstract Fluorescence nanoscopy refers to the experimental techniques and analytical methods used for fluorescence imaging at a resolution higher than conventional, diffraction-limited, microscopy. This review explains the concepts behind fluorescence nanoscopy and focuses on the latest and promising developments in acquisition techniques, labelling strategies to obtain highly detailed super-resolved images and in the quantitative methods to extract meaningful information from them.

Keywords Super-resolution · Fluorescence nanoscopy · Subdiffraction imaging · STED · STORM · PALM · SIM

Abbreviations

3B	Bayesian analysis of the bleaching and blinking
βME	β-Mercaptoethanol
φ_{Fl}	Fluorescence quantum yield
AChR	Acetylcholine receptor
BaLM	Bleaching/blinking assisted localisation microscopy
CHO	Chinese hamster ovary
CW	Continuous wave
*d*STORM	Direct STORM
EM	Electron microscopy
ER	Endoplasmic reticulum
EMCCD	Electron-multiplying CCD
FCS	Fluorescence correlation spectroscopy
FIONA	Fluorescence imaging with 1 nm accuracy
FlAsH	Fluorescein arsenical helix
FP	Fluorescent protein
FPALM	Fluorescent photoactivation light microscopy
FWHM	Full width half maximum
GPI	Glycophosphatidylinositol
GSH	Glutathione
GSD	Ground state depletion
GSDIM	Ground state depletion followed by individual molecule return
GPU	Graphics processing unit
HA	Hemagglutinin
HIV-1	Human immunodeficiency virus type 1
LM	Localisation microscopy
MEA	Mercaptoethylamine
MLE	Maximum likelihood estimate
NA	Numerical aperture
NK	Natural killer
NPC	Nuclear pore complex
PA-FP	Photoactivatable fluorescent protein, it is usually referred to any photoactivatable, photoswitchable or photochromic FP
PAINT	Paint accumulation for imaging in nanoscale topography
PALM	Photoactivation localisation microscopy
PALMIRA	Photoactivation light microscopy with independent running acquisition
PIP2	Phosphatidylinositol 4,5-bisphosphate
PSF	Point spread function
RESOLFT	Reversible, saturable, optical fluorescence transition
SIM	Structured illumination microscopy
SOFI	Stochastic optical fluctuation imaging
SSIM	Saturated structured illumination
STORM	Stochastic optical reconstruction microscopy
STED	Stimulated emission depletion
TCR	T cell antigen receptor
TfR	Transferrin receptor
TIRF	Total internal reflection fluorescence

J. Requejo-Isidro (✉)
Unidad de Biofisica, CSIC-UPV/EHU,
Barrio de Sarriena, s/n., 48940 Leioa, Spain
e-mail: j.requejo@csic.es

Introduction

Far-field fluorescence microscopy is one of the key tools for the understanding of cell architecture and function: It allows

molecules to be observed in two and three dimensions and to be followed in time and space with single molecule sensitivity and high specificity. However, the smallest detail that can be resolved with a conventional microscope is limited to around 200 nm. Recent years have seen the development of methods that overcome this constraint.

The outline of this review is as follows: First, the working principles of the main fluorescence nanoscopy methods and their variations are presented highlighting their temporal resolution and its implications for live-cell imaging. Next, relevant aspects of the properties and the photophysical behaviour of fluorescent probes suitable for nanoscopic imaging are explained. A discussion on the meaning of resolution follows before reviewing the most recent developments in analytical tools for quantitative description of molecular organisation at the nanoscale. Finally, prominent applications of light nanoscopy in the areas of biology on which this technique is having a significant impact are presented (Table 1).

The diffraction limit

Light exhibits properties of both waves and particles: Its wave nature means light is subject to diffraction, a physical phenomenon that underlies the fact that it cannot be focused to an infinitely small spot, but, rather, to a spot roughly half a wavelength wide. Conversely, diffraction is also responsible for the spatial intensity distribution that is observed when a point-like emitter, such as a single fluorescent molecule, is imaged through a microscope (Fig. 1 a). This spatial distribution is called the point-spread function (PSF) and its width is commonly used as a measure of the resolution of the imaging system. As the image of an object, such as a fluorescently labelled cell, is equivalent to the superposition of the images of the point-like emitters composing the extended object, diffraction limits the smallest discernible detail and, therefore, resolution.

Resolution is, in a general sense, defined as the minimum separation between two point objects such that they can still be distinguished (Fig. 1 b–d). There is some ambiguity as to what this minimum separation is, but it is broadly assumed that two objects are resolvable (in the lateral and axial dimension, respectively) if they are at a distance larger than (Sparrow resolution criterion):

$$r_{x,y} \approx \frac{0.5\lambda}{\mathrm{NA}} \qquad r_z \approx \frac{2n\lambda}{\mathrm{NA}^2} \qquad (1)$$

where λ is the wavelength of the light, n the index of refraction of the medium, and NA the numerical aperture of the lens (incidentally, $r_{x,y}$ and r_z are the radii of the mathematical function that describes the PSF of the lens [1]). For visible light and high-NA objective lenses, diffraction limits the lateral resolution to ≈200 and to ≈550 nm in the axial dimension. Optical microscopy at higher resolution is termed super-resolution, subdiffraction imaging or nanoscopy. Although it is frequently overseen, the inherent properties of the specimen and the way it has been labelled also restrict the achievable resolution: Fluorophores may bleach or labelling may be too sparse; besides, living specimens are subject to phototoxicity which restrict the power of the incident light and thick samples distort the profile of the incident beam degrading resolution.

Principles of light nanoscopy

Optical nanoscopy based on the reduction of the fluorescently emitting region. STED, GSD and RESOLFT

Concept

Subdiffraction resolution can be achieved by temporarily preventing fluorophores in the outer range of the focal spot from fluorescing, reducing, therefore, the emitting volume to a region smaller than the diffraction-limited focal spot. When this spot of subdiffraction dimensions is scanned across the specimen, a super-resolution image is obtained. Subdiffraction imaging techniques that share this working principle are termed reversible saturable optical transition (RESOLFT) [2]; depending on the particular molecular transition exploited to switch fluorophores to a dark state, the modalities are termed stimulated emission depletion (STED) [3–5], ground stated depletion (GSD) [6, 7] or, simply, RESOLFT [8].

STED

Stimulated emission depletion microscopy [3–5] relies on exciting all fluorophores within the focal spot and immediately driving those lying in the periphery of the focus back to the ground state through stimulated emission by an additional lower energy photon, leaving the spot centre unaffected. This way, fluorophores in the central region are allowed to spontaneously decay, and fluorescence emission can be unambiguously assigned to this small region.

Stimulated emission is a process whereby an excited molecule interacts with a photon and drops to a lower energy level emitting a second photon of identical wavelength, phase, polarisation and direction as the incident photon. In a STED experiment, the excitation beam is overlapped with a lower wavelength torus-shaped beam (depletion or STED beam, see Fig. 2, left and middle) that provides the additional photons required for stimulated emission: Excited molecules in the overlap region undergo stimulated emission. Hence, they decay to the ground state in a controlled manner and do not participate in image formation, while those in the central region will eventually emit a fluorescent photon with the characteristic

Table 1 Summary of nanoscopy methods

Description	Type of fluorophores	Relevant references
RESOLFT		
STED		
Fluorophores in the outer region of the focal spot are controllably driven to the ground state by stimulated emission immediately after excitation, confining spontaneous emission to the central subdiffraction-sized volume	Certain organic dyes and fluorescent proteins	[5, 10, 11, 13]
RESOLFT based on photoswitching fluorescent proteins		
PA-FPs in the outer region of the focal spot are controllably photodeactivated, confining spontaneous emission to the remaining active fluorescent proteins, located in the central subdiffraction-sized volume	Certain photoswitchable fluorescent proteins	[23, 24]
GSD		
Fluorophores in the outer region of the focal spot are controllably driven to a stable dark (triplet) state through high-intensity excitation, confining emission to the central subdiffraction-sized volume	Certain organic dyes in suitable red-ox conditions	[6, 7]
Stochastic localisation microscopy		
PALM		
Fluorescent proteins in a sample are individually photoactivated and precisely localised in a sequential manner until the image of the sample is reconstructed	Photoactivatable, photoswitchable or photochromic fluorescent proteins	[34, 36]
*d*STORM, GSDIM		
Fluorophores under suitable chemical conditions are individually activated and precisely localised in a sequential manner until the image of the sample is reconstructed	Certain organic dyes in suitable red-ox conditions	[35, 38, 39]
Single particle tracking PALM		
Maps the trajectories of single molecules at high molecular density. An outline of the accessible volume is obtained as well as biophysical parameters (e.g. diffusion)	Photoswitchable fluorescent proteins	[41]
PAINT		
The surface of a cell is transiently labelled with a synthetic dye that becomes fluorescent upon binding	Certain synthetic dyes	[42]
SOFI, BaLM and 3B analysis		
Statistical analysis of the spontaneous intensity fluctuations of fluorophores as a function of time (blinking) allows their localisation	Certain organic dyes and photoswitchable proteins	[90, 92, 94]
SIM		
SIM		
Patterned excitation allows information on fine details in the sample to be modulated onto the emitted pattern. Upon detection, the pattern is demodulated and the fine details are recovered. Resolution is limited to twice the resolution of diffraction-limited microscopy	Most fluorophores	[100]
Nonlinear SIM or sSIM		
Nonlinear molecular behaviour is exploited for improved SIM resolution	Photoswitchable proteins	[103]

lifetime of the unperturbed fluorescent transition (Fig. 2, right). Careful timing of excitation, stimulated emission of the focal spot periphery and detection result in detection of photons that have originated in the small central region. The net result is a subdiffraction-sized spot of diameter on the *x*–*y* plane:

$$d \approx \frac{\lambda}{\mathrm{NA}\sqrt{1+\frac{I_{\max}}{I_{\mathrm{sat}}}}} \qquad (2)$$

where $I_{\max}$ denotes the peak intensity of the depletion beam and I_{sat} the characteristic intensity required to efficiently induce stimulated emission of the excited fluorophore. Adjusting $I_{\max} \gg I_{\mathrm{sat}}$ allows the resolution to be tuned to molecular scale; for arbitrarily large $I_{\max}/I_{\mathrm{sat}}$ resolution is theoretically unlimited (Fig. 2, middle); in practice is limited by photodamage to the sample and the photostability of the fluorophores. Lateral resolution of STED images of biological samples typically varies between 30 to 80 nm, while resolution down to 5.8nm has been demonstrated on inorganic structures [9]; axial resolution is on the order of 100 nm [5]; a complex combination of 4Pi and STED imaging has achieved a 3D isotropic resolution of 45 nm on biological samples [10] (Fig. 3).

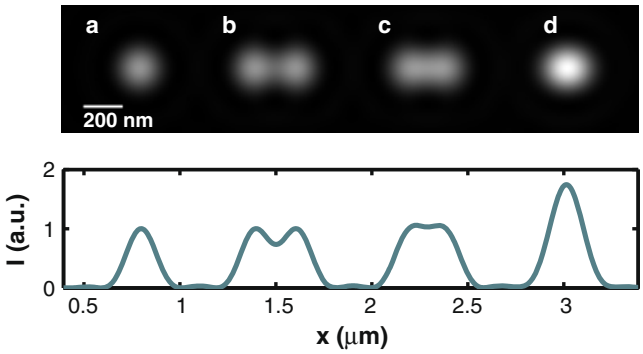

Fig. 1 Resolution criteria for λ=500 nm and NA=1.47. *a* An isolated molecule as seen through a conventional fluorescence microscope; *b* two molecules 207 nm apart (Rayleigh criterion); *c* two molecules 170 nm apart (Sparrow criterion—Eq. 1); *d* two molecules 80 nm apart (unresolved). The *bottom panel* shows the intensity profile of the molecules above

Resolution of STED microscopy scales as the inverse square root of the depletion beam intensity I_{max} (Eq. 2; ≈1 GW cm^{-2} is required for 65 nm lateral resolution). Pulsed lasers with ps- or fs-pulse duration deliver very high peak power and allow synchronicity control between the excitation and depletion pulses, which is the reason why they were preferred in STED first implementations. However, the high laser intensities required for STED imaging affect the photobleaching rate of fluorophores in the specimen and may induce phototoxicity not only in the image plane, but also in the light cone above and below the focal spot. Besides, a fluorophore can only be excited once per lifetime; therefore, with interpulse time intervals much longer than the chromophore lifetime (as is usually the case), fluorophores are mostly in an idle state. An alternative to pulsed lasers are high power continuous wave (CW) lasers: These lasers deliver an uninterrupted stream of photons, such that a molecule can be excited as soon as it is in its ground state without the need for waiting for the arrival of the next laser pulse. Photons can, therefore, be emitted constantly with an average of about one per lifetime: The use of CW lasers that provided enough power for CW-STED would thus result in more efficient STED and simpler experimental setups [11]. The drawback is that, unlike in pulsed STED, in which excitation and depletion occur sequentially, CW-STED is compromised by ongoing excitation, which results in a less pronounced on-off contrast and, consequently, lower resolution. Combining

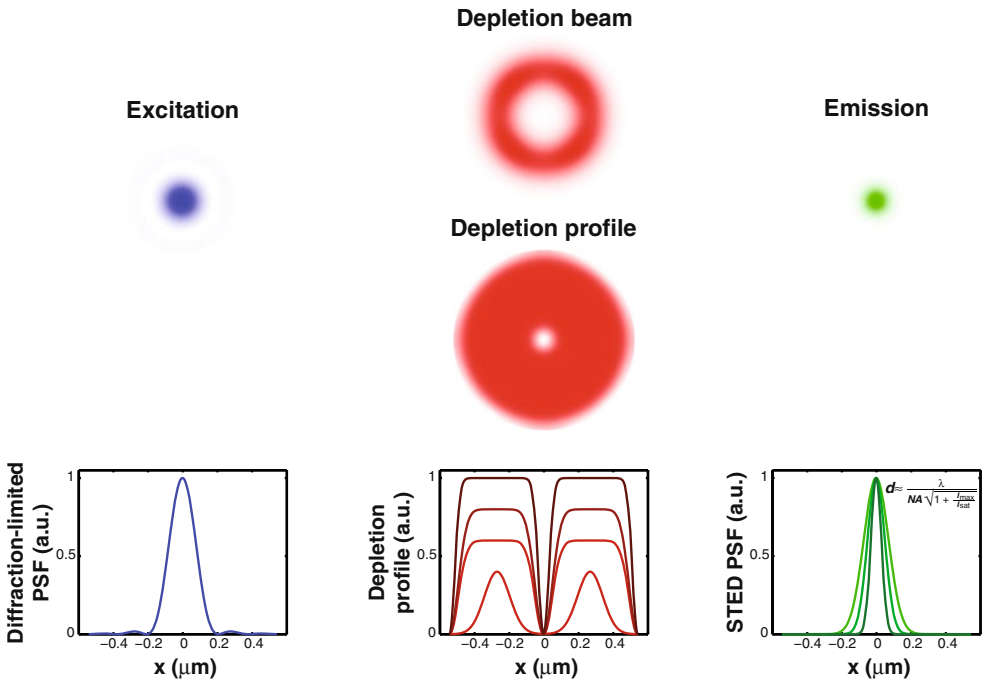

Fig. 2 STED working principle: First, molecules within the diffraction-limited focal spot are excited (*left*). Before fluorophores are allowed to spontaneously decay to the ground state, a red-shifted torus-shaped beam (depletion beam) induces stimulated emission of the molecules at the periphery of the focal spot (*top*, *middle*); as the peak intensity I_{max} of the depletion beam increases beyond saturation of the stimulated emission, I_{sat}, the depleted region gets larger (*middle*) and the undepleted central spot is reduced as a result. Molecules that have undergone stimulated emission are now in their ground state and, hence, cannot fluoresce. Finally, the small central region spontaneously decays with the characteristic lifetime of the fluorescent transition (*left*), which is read out and assigned to the spatial position of the scanning beam. The *bottom row* shows the excitation PSF, the depletion profiles for increasing I_{max} and the resulting PSF (note that for $I_{max} < I_{sat}$, shown in *bright red colour*, there is no gain in resolution and the corresponding PSF is identical to the conventional PSF). Likewise, RESOLFT based on photoswitching fluorescent proteins saturates the molecular transition that deactivates the FP in order to restrict the active region to subdiffraction dimensions

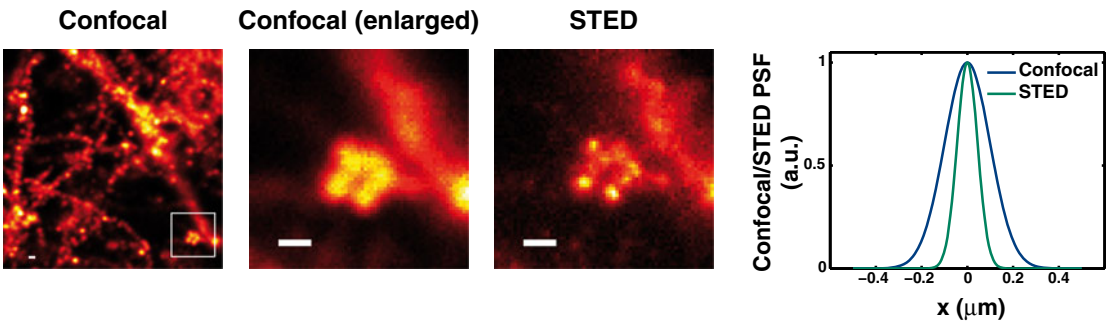

Fig. 3 Example of a STED image of a primary culture of rat cortical neurons labelled with Alexa 488-tagged IP_3 (inositol 1,4,5-trisphospate) receptor specific antibodies. The *rightmost graph* shows the confocal and STED actual PSFs, with FWHM 233 and 106 nm, respectively. *Scale bars* are 300 nm in all three images

pulsed excitation with a CW-depletion beam and time-correlated single photon counting detection (gated STED or g-STED) solves this problem allowing synchronicity between excitation and detection. g-STED has been demonstrated to provide the same resolution with ten times lower depletion intensities (≈0.1 GW cm^{-2}) than pulsed STED [12, 13].

Multicolour STED allows nanoscopic imaging of differently tagged specimens in the same sample. Dual-colour STED has been demonstrated employing separate excitation and depletion beams for two fluorophores (making a total of four beams) [14], using separate excitation beams but the same depletion beam for both fluorophores [10] or, even, a single excitation beam and a single depletion beam with a particular combination of photoswitchable fluorescent proteins (Dronpa and Padron) [15]. Fluorescence lifetime has also been used to discriminate up to three fluorophores in a STED image [16].

The main application of STED has been structural imaging, but the reduction of the excitation volume results in a decreased number of fluorophores diffusing through that volume, which is advantageous for the investigation of molecular mobility and interactions by fluorescence correlation spectroscopy (FCS) [17–20]. FCS is a technique that allows the diffusion coefficient of a molecule to be determined from the analysis of the fluctuations of its fluorescence emission as it traverses a known volume: The lower the number of fluorophores within the focal volume, the more accurate the measurements. Also, fluorescence lifetime imaging with subdiffraction resolution has been demonstrated on a STED microscope [21], paving the way for functional nanoscopy.

RESOLFT based on photoswitching fluorescent proteins

The reversible switching behaviour of photoswitchable proteins can also be exploited to confine fluorescence to a subdiffraction-sized spot with the important advantage that the power needed to activate and deactivate fluorescent proteins is much lower than that required for depletion by stimulated emission: A diffraction-limited focal intensity distribution featuring a central intensity zero deactivates all photoswitchable fluorescent proteins on the periphery of the spot leaving the small central region activated. Only those fluorophores in this subdiffraction-sized active region can subsequently be excited; hence, fluorescence is assigned unequivocally to that small spot [8, 22]. Akin to STED, the size of the subdiffraction spot in RESOLFT imaging is determined by Eq. 2, with I_{sat} referring to the intensity required to efficiently photoswitch the fluorophore to a dark state. RESOLFT based on photoswitching fluorescent proteins has been limited for many years by the slow photokinetics of most fluorescent proteins, but recently developed fluorescent probes and experimental designs allow faster RESOLFT at low intensities (1 W cm^{-2}) [23, 24].

Ground state depletion

Optical shelving or GSD imaging [6, 7] is another super-resolution imaging technique based on the RESOLFT concept: Molecules in the periphery of the focal spot are driven to the lowest triplet state (optical shelving) depleting the fluorophores ground state and transiently confining the fluorescence emission to the unaffected central spot of subdiffraction size. In practice, recovery of the fluorescence is essential as the technique relies on scanning. The challenge is to avoid irreversible photobleaching due to photoionisation and reaction with molecular oxygen while the molecule is in a dark state [25], which accounts for the fact that GSD had been suggested [6] more than a decade before it was demonstrated [7], when the conditions for optical shelving compatible with scanning microscopy (microsecond-long transient shelving) were eventually established.

Temporal resolution and live-cell STED/RESOLFT imaging

The time and power required to produce an image limit the applicability of imaging techniques to the study of living cells. STED is a scanning technique and hence its speed is determined by the scanning mechanism and the size of the area to be scanned. Increasing scanning speed requires excitation and

depletion powers to be increased accordingly, and therefore, photodamage and photobleaching become a major concern. Video-rate (28 Hz) STED imaging at 65 nm lateral resolution has been demonstrated on living cells, although the field of view was relatively small (4.5 μm^2), and it was confined to two dimensions possibly due to out-of-focus photodamage, which precluded from whole-cell imaging [26, 27]. In an impressive demonstration, in vivo STED of the brain of a living mouse has been recently demonstrated [28].

STED live-cell imaging can be performed using synthetic fluorophores, which are advantageous as they are brighter and more photostable than fluorescent proteins. Besides being permeable to the plasma membrane, tagging intracellular proteins with synthetic fluorophores requires genetically encoded labelling systems (see "Probes and labelling systems" section). Using SNAP- and CLIP-tag labelling technologies, dual-colour live-cell STED imaging was demonstrated at ≈80 nm resolution [29].

RESOLFT based on photoswitchable fluorescent proteins is, however, the most promising modality as intensity levels required for activation and deactivation are far lower than those required by STED. Progress in this area will go hand in hand with the development of photoswitchable proteins with faster photokinetics [23, 24].

An alternative strategy to increase imaging speed is to parallelise the excitation and depletion beams. Such an approach was demonstrated in 2011, using four excitation and depletion beams attaining a ×4 increase in acquisition speed (STED imaging) [30].

Localisation microscopy

Whereas the resolution of conventional optical microscopy is limited by diffraction, isolated emitting molecules can be localised within a region much smaller than the diffraction-limited volume (Fig. 4). Localisation of a molecule refers to the mathematical determination of its position from an image: If the PSF of the imaging system has been previously characterised, molecules can be localised to a precision, σ_{loc}, that depends on the number of photons that have been detected and is much higher than the width of the distribution, σ_{PSF} [31]:

$$\sigma_{loc} = \frac{\sigma_{PSF}}{\sqrt{N_{phot}}} \quad (3)$$

where N_{phot} is the number of detected photons. A super-resolved image may thus be obtained upon subdiffraction localisation of all the molecules in the sample and subsequent rendering at their coordinates (Fig. 5). As molecules in biological samples are, in general, not isolated, but in very close vicinity of one another, their emission needs to be temporally isolated in a way that molecule identification and localisation in the sample ensemble is feasible. Multiple strategies have been put forward; all share the same principle of sparsely and stochastically driving fluorophores to molecular states with different emission properties to reduce the overlap of their intensity distributions and, thus, allow precise localisation of individual molecules. These techniques have received multiple names based on the mechanisms they exploit for isolating or localising the molecules; they are collectively known as pointillist or stochastic localisation microscopy (LM). It is worth noting that localisation precision is not equivalent to resolution: The resolution achieved with LM strategies depends very much on the available photons, but also on the labelling density and the experimental configurations. For biological samples, it is generally around 20 nm in the lateral dimension (up to ≈4 nm [32]) and around 70 nm in the axial dimension (up to ≈6 nm [33]).

Nanoscopy based on molecular photoswitching light microscopy: PALM, STORM, FPALM, PALMIRA, GSDIM, sptPALM and PAINT

Localisation microscopy-based nanoscopy was demonstrated simultaneously by three groups in the summer of 2006 [34–36]. Each group gave the technique a different name based on the molecular mechanism used to activate a low density of emitters simultaneously: photoactivation localisation microscopy (PALM) [34] and fluorescence photoactivation localisation microscopy (FPALM) [36] make use of photoconvertible fluorescent proteins that are converted from one fluorescent state (inactive) to another (active) with a UV pulse while imaging at a longer wavelength; stochastic optical reconstruction microscopy (STORM) [35] exploits the photoswitching properties of tandems of closely spaced inorganic tags (such as Cy5–Cy3). STORM can also be performed on standard inorganic fluorophores (such as Cy, Alexa or Atto dyes) that can be switched to a reversible metastable nonemitting state using

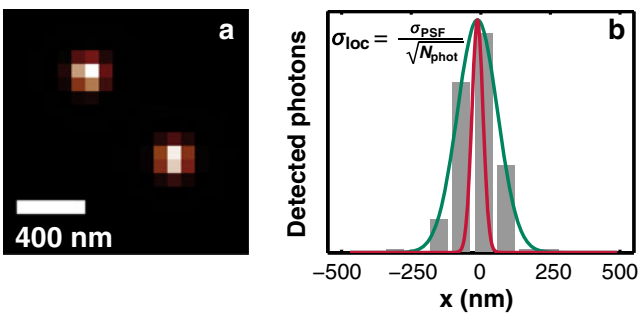

Fig. 4 The position of spatially isolated molecules (**a**) is determined from the intensity of their emission pattern in each pixel (in *grey* in **b**). The localisation precision, σ_{loc} (in *red*), is dependent on the number of photons that have been detected and is much higher than the standard deviation of the intensity distribution of the emitter σ_{PSF} (PSF, shown in *green*)

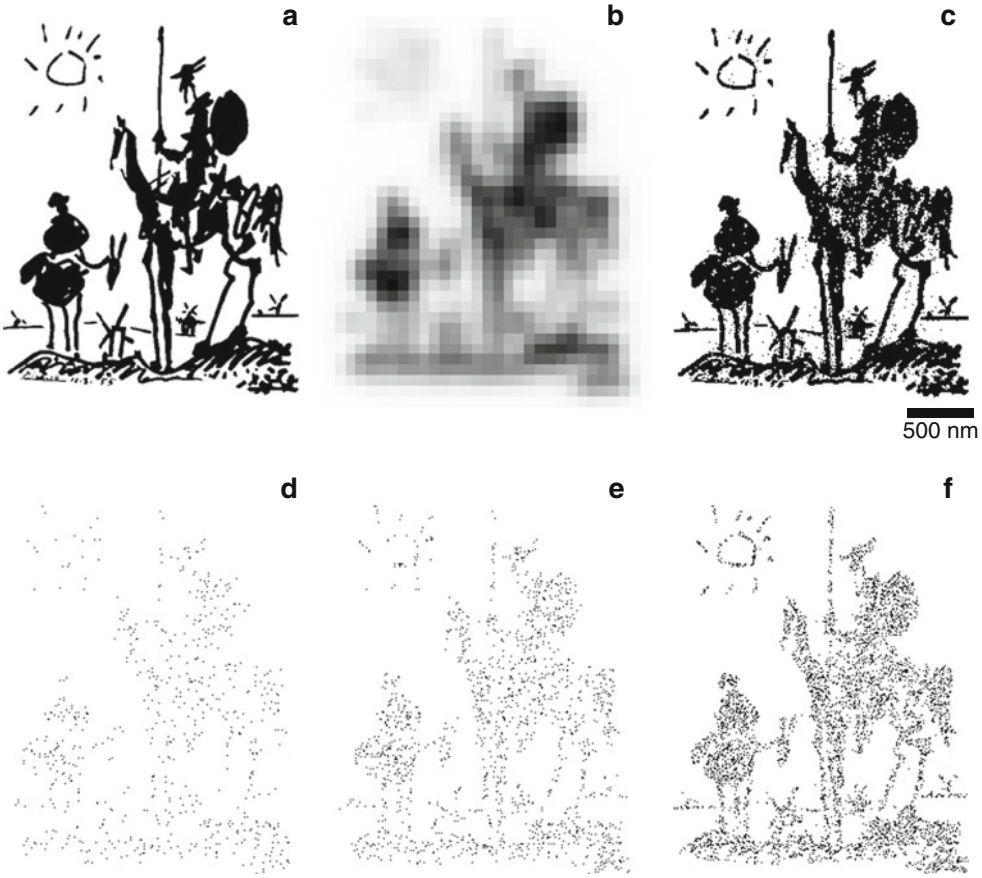

Fig. 5 Picasso's 1955 Don Quixote illustrates stochastic localisation microscopy (**a**–**c**) and the effect of labelling density on resolution (**d**–**f**): A molecular Don Quixote has been simulated as a collection of ≈54,000 5-nm-round fluorophores (**a**). When observed through a diffraction-limited microscope, the drawing appears pixelated and even the knight of doleful countenance is hardly distinguishable (**b**). Reconstruction has followed PALM procedure for molecule activation, identification and localisation at ≈20 nm localisation precision (**c**). **d**–**f** Partial steps of the reconstruction at ≈700, 1,700 and 6,000 identified molecules. Note the effect of labelling density: Details on windmills and the sun, for instance, are lost at low labelling density (**d**, **e**). Irrespective of the localisation precision, labelling density sets a limit to the achievable resolution

relatively high intensity illumination (≈10 kW cm^{-2}) under suitable chemical conditions and subsequently photoinduce their activation or let them activate spontaneously. This variation of STORM has been termed direct STORM (*d*STORM) [37, 38]), ground state depletion followed by individual molecule return (GSDIM) [39] or, simply, STORM. The microscope arrangement for PALM and STORM is very similar, involving in its more general form a UV activation laser (usually at 405 nm), a visible excitation laser and an EMCCD for sensitive imaging of individual molecules. Photoinduced activation may not be necessary: PALM with independently running acquisition (PALMIRA) exploits spontaneous activation and deactivation and asynchronous detection, which results in faster acquisitions [40].

When the interest is restricted to imaging the cell membrane, single particle tracking of photoswitchable fluorophores (sptPALM) and transiently labelling the surface with synthetic dyes that become fluorescent upon binding (point accumulation for imaging in nanoscale topography, PAINT) are two variations of stochastic LM that achieve higher number of localisations: sptPALM allows hundreds of individual molecules to be visualised and localised at the same time with tens of nanometres precision, mapping the trajectories of single molecules at high molecular density [41]; PAINT involves transiently labelling the surface of the cell such that a fluorescent signal appears as a diffraction-limited spot when the fluorophore binds to the membrane and disappears when it dissociates or bleaches [42–44]. PAINT and sptPALM are advantageous over conventional single particle tracking because many overlapping trajectories can be followed as long as the distance between fluorescent molecules at any time is greater than several times the width of their PSF. But beyond the single molecule information on biophysical parameters such as diffusion, sptPALM and PAINT allow super-resolution images of the cell morphology to be obtained at an effective very high labelling density as the individual fluorophore trajectories outline the accessible cell volume.

Nanoscopic imaging of multiple fluorophores in the same sample (multicolour PALM or STORM) based on the different emission or activation wavelength was readily achieved after these techniques had been first demonstrated with either two or a single imaging wavelength [45–49]; up to four fluorophores can be discriminated with these strategies [50, 51]. Combinatorial pairing of photoswitchable tags with fluorophores that enhance photoactivation enabled subdiffraction multiparameter detection of six different probes [52]. Although the preparation of biological samples with six fluorescent probes is challenging, this report demonstrated that observation of multiple targets at nanometre resolution and molecular specificity is feasible.

Stochastic localisation microscopy in 3D

Localisation microscopy is generally performed using wide-field illumination. This configuration hampers super-resolution imaging in the three dimensions as molecules are activated throughout the whole sample: Activated molecules outside the focal plane will fluoresce upon absorption of a photon from the excitation beam contributing to an out-of-focus background which degrades localisation precision. This is the reason why most LM experiments are based on a TIRF configuration, which constrains imaging to a thin sheet of less than 100 nm contiguous to the coverslip.

Several strategies have been put forward to achieve three-dimensional localisation microscopy: biplane detection [53], astigmatic imaging [54], engineered PSFs whose profiles unambiguously change with depth [55–57], confined two-photon activation [58–60], interferometric PALM (iPALM) [61] and highly inclined and laminated optical sheet illumination [62].

The first three are of particular interest because they require only minor modifications of a standard microscope and operate in moderate depth ranges: Biplane detection and astigmatic imaging extract depth information from the analysis of the image pattern of each molecule when it is subject to defocus or astigmatism, while imaging the sample with an engineered PSF beam that propagates axially as if it was following a double-helix pattern allows depth information to be extracted from the relative spatial position of the maxima at each plane. Among these strategies for 3D localisation, the double-helix PSF along with an optimised localisation algorithm offers better axial localisation precision (≈20nm) over an extended depth range (over 2 μm) than the astigmatic PSF or biplane imaging (≈65 nm) [63, 64].

Akin to two-photon fluorescence excitation diffraction-limited microscopy, nonlinear activation of a thin optical section can be induced by a pulsed IR beam (confined activation). The activating IR beam can either follow the excitation path so that the same objective is used for activation, excitation and detection [58, 59] or be relayed to the sample through an objective for activation and excitation set in an orthogonal configuration to a second, imaging, objective (selective plane illumination regime, SPIM [65]). Confined nonlinear activation is advantageous for nanoscopic depth imaging of whole cells and thicker samples such as spheroids (SPIM configuration [60]).

Superb lateral and axial resolution (≈4 and 5.4 nm, respectively [32, 33]) has been achieved sandwiching the sample between two objectives to exploit the self-interference of emitted photons while taking advantage of the extra budget of photons available for improved localisation in all directions (interferometric PALM, iPALM or 4Pi-LM) [32, 33, 61]. This approach is limited to a 1-μm-thick optical layer (although the sample can be thicker) and is constrained by the severe complexity of the experimental setup.

Algorithms for precise localisation

PALM imaging relies heavily on algorithms for molecule identification and ensuing localisation. These algorithms must be able to identify individual molecules that are in close proximity and localise them with nanometre precision in a period of time compatible with the experiment. The computational effort required by this task is tremendous: A typical PALM image has a field of view of 50×50 μm^2 and requires localisation of around 10^6 molecules; the background may vary across the field of view, and the emission rate of chemically identical fluorophores can also vary due to poor photostability, uneven illumination profile, dipole orientation or different optical path lengths.

Several solutions to the problem of localising a single fluorescent molecule with subdiffraction accuracy have been proposed, either based on fitting the measured intensity profile of each emitter to a two-dimensional Gaussian PSF or on algebraic solutions, such as centroid localisation, the fluoroBancroft algorithm [66] or the exploitation of the radial symmetry of the emitter intensity distribution [67, 68]. Some of these algorithms are freely available as standalone software (LivePalm [69], rapidStorm [70]) and ImageJ plugins (QuickPalm [71]).

Among these, maximum likelihood estimation (MLE) of the position of the emitter achieves the minimal theoretical uncertainty [72, 73]. The drawback is that iterative algorithms are highly computationally demanding and the reconstruction of the subdiffraction image at the time is being acquired requires careful optimisation of the algorithms [70] or implementation on GPU architectures [73, 74]. Algebraic solutions to localising individual molecules are inherently faster as they do not rely on iterating procedures, but their precision is, in general, lower. Among them, calculation of radial symmetry centres outperforms nonlinear least squares minimisation and gets closer to the precision reached by MLE methods [67]. It is worth noting that all localisation algorithms have been developed under the assumption of freely rotating dipole emitters imaged through unaberrating optics or with symmetric aberrations, such as defocus or spherical aberration. Under these conditions, the PSF is isotropic and resembles a Gaussian model, but accuracy drops significantly for emitters which are not allowed to rotate (on the order of 50 to 100 nm) [75], in particular in 3D PALM imaging [76, 77]. Recent works are considering the effect of the orientation of molecules on localisation [72, 77, 78]. It is worth noting that STED is also affected by molecular orientation, but being a scanning technique, the read-out position is predefined by the zero of the depletion distribution and therefore the effect of molecular orientation is smaller.

Stochastic LM acquisitions usually take tens of seconds to minutes, which turns the measurement prone to sample drift that degrades resolution. The positions of localised fiduciary

markers that do not bleach, such as small gold beads added to the sample, can be used to compensate for the drift or, if the sample has static structures, subpopulations of molecules in different frames during the acquisition can be correlated [79]. A fully data-driven statistical registration method for drift detection and correction has also been proposed [80].

Temporal resolution and live-cell stochastic LM

Live-cell stochastic LM is severely limited by a relatively poor temporal resolution (tens of seconds to minutes in its most common implementation), which is determined, in turn, by the need for acquisition of several thousands of frames where only a subset of probes are active (usually around 15,000 frames). Switching rates can be increased (and, therefore, the acquisition time decreased) through simultaneous activation, excitation and detection, matching the detection time to the lifetime of the fluorophore active state [40, 81] and also using higher excitation powers. This strategy has allowed STORM imaging at the remarkable speed of 0.5 s at ≈25 nm resolution [82]; however, high excitation power results in degradation of the fluorescent signal from some of the most frequently used photoswitchable proteins [82] and induce nonphysiological changes in living cells (at more than 1 kW cm^{-2} [83]).

A different strategy for speeding stochastic LM acquisition up is to increase the number of localised molecules per frame: Localisation of a large number of molecules is essential to LM imaging as the resolution limiting factor in localisation microscopy is usually the labelling density and not the localising precision. The time needed to image a densely labelled structure is, in turn, limited by the number of molecules that can be concurrently active and properly identified: Multiple molecules which reside within one diffraction-limited area may be misidentified as one single molecule, limiting the density of active molecules to less than 1 molecule/μm^2: A comparison of the performance of commonly used localisation algorithms reported that the density of active fluorophores should be adjusted below 0.5 fluorophore/μm^2 to minimise false identifications and maximise the number of localisations [84]. High-speed imaging registers a lower number of photons per molecule that hinders molecule identification, and thus, the density of active fluorophores per frame must be reduced even further (e.g. down to 0.01–0.03 fluorophore/μm^2 imaging at 3.3 Hz [85]).

As the number of localised molecules per frame increases, the number of frames required to reconstruct the whole image is lower, and the total acquisition time is reduced accordingly. Proper identification and precise localisation of molecules with overlapping PSFs have recently been demonstrated, even though it is still challenging: Algorithms for multiple-emitter fitting and residuals image analysis have been successfully applied to localisation microscopy, allowing molecules to be identified in an image with a density of active fluorophores of 10 molecules/μm^2, one order of magnitude higher than sparse single-molecule localisation algorithms [86, 87]. Accordingly, the number of frames required for reconstruction of an image is reduced by a factor of 10 as compared to single-emitter fitting. An alternative strategy that has recently been demonstrated for LM imaging is known as compressed sensing, a signal processing technique used for signal recovery from highly noisy or corrupted measurements that allows 15 times more molecules to be identified than single-molecule fitting approaches (up to a density of 8.8 molecules/μm^2) [88]. Compressed sensing allowed a super-resolution image to be reconstructed from only 200 frames, requiring just a 3-s acquisition at 60 nm resolution [88]. The immense computational effort these algorithms perform demands their implementation on GPU architecture.

Methods based on the statistical analysis of fluorophore blinking have also proved very successful for molecular localisation in high molecular density images with improved temporal resolution [89–92]. These methods are described below as they make use of different spectroscopic properties.

Rather than increasing the density of active molecules per frame, a different approach aims at reducing the acquisition time by reducing the number of identified fluorophores, inferring biological structures from undersampled super-resolution LM images using generative models [93].

SOFI, BaLM and Bayesian localisation methods

Three novel strategies have been recently proposed for the extraction of a super-resolution image from recording the spontaneous fluorescence intensity fluctuations as a function of time in each pixel: stochastic optical fluctuation imaging (SOFI) [89, 90], bleaching/blinking assisted localisation microscopy (BaLM) [94] and Bayesian analysis of the blinking and bleaching (3B analysis) [91, 92]. All methods rely on recording a stream of high fluorophore density images while continuously exciting the fluorophores; each fluorophore can emit light but not necessarily in each recorded image (due to inherent blinking). The spatial resolution achieved with these strategies is similar (50 to 60 nm), slightly lower than PALM-based techniques, but with a much simpler setup than standard PALM systems and better temporal resolution: SOFI has reported a two-fold increase in resolution upon reconstruction from only 1,000 frames [89], and 3B analysis has reported 50 nm resolution from only 300 frames, which can be collected in just 6 s [92].

SOFI and 3B analysis are based on the statistical analysis of the intensity fluctuations of fluorophores (blinking) in each pixel as a function of time while BaLM relies on subtraction of contiguous frames and subsequent PALM/STORM-manner localisation. These methods are technically much simpler than PALM or STORM for they exploit the inherent blinking

behaviour of fluorophores as they are subject to continuous excitation and therefore there is no need for activation and bleaching. As virtually all fluorophores show blinking cycles, these approaches allow, in principle, the use of standard fluorescent fluorophores as long as fluctuations are sufficiently slow to be resolvable compared to the acquisition time (tens of milliseconds in practice). So far, the use of Alexa Fluor dyes and Dronpa-tagged proteins has been demonstrated. Dual-colour and 3D SOFI [89] has been reported as well as multicolour BaLM [94] and 3D, 3B analysis [92]. Accelerating 3B analysis through widely accessible cloud computing has been recently reported [95].

Visualisation and rendering

In epifluorescence or confocal microscopy as well as STED or SIM nanoscopy, the intensity of each image pixel is proportional to the number of photons registered at that pixel. However, LM data are not an image but a list of discrete coordinates of the estimated position of the molecules that needs to be converted into an image. The straightforward conventional way of representing LM data is to force molecules onto a regular grid, binning molecular positions into pixels with an intensity proportional to the number of localised molecules in that area (i.e. a 2D colour-coded histogram). In an effort to convey the uncertainty of the localisation procedure, molecule positions may also be rendered as a 2D Gaussian distribution. However, the former methods suffer from nonlinearity and loss of resolution and result in spurious structures as resolution in LM microscopy is dependent on both localisation precision and labelling density. The Soeller group has proposed rendering methods based on triangulation and 2D histograms with labelling density-dependent bin-size to reduce artefacts in poorly sampled images and convey information on data quality (resolution and noise) [96]. With a similar aim, Krizek et al proposed to randomly shift molecules around their localisation position within the localisation accuracy, effectively blurring the localised position based on the localisation precision [97].

SIM and nonlinear SIM

Concept of SIM. Nonlinear SIM

Sound and electromagnetic waves can be described as a sum of their frequency components: a series of sine and cosine waves that, when added with the appropriate amplitude, allows the original wave to be reproduced. In a similar fashion, an image is the sum of its spatial frequency components. The amplitude variations in time of a sound wave are analogous to the intensity variations in space of an image: Low spatial frequencies are associated with slow variations of the intensity in an image, such as the ones found in a blurred image; high spatial frequencies are associated with steep intensity variations, such as the sharp contrasted edges that are found in highly detailed structures.

Optical systems only allow certain frequencies to go through them; as fine detail in an image is associated with higher frequencies, the higher the frequency relayed to the detector (CCD, eye etc.), the higher the resolution of the image. Spatial frequencies that are not relayed by the optical system are attenuated. However, if the high-frequency components of an image, f_h, are offset by a known amount, Δf, to a lower frequency f_l, then after detection they can be offset back by the same amount to its former value, $f_l+\Delta f=f_h$. This is the basis of structured illumination super-resolution microscopy[1] (SIM): Fine details in the sample contain high frequencies f_h that cannot be relayed by the microscope objective (and therefore cannot be imaged) but can be offset to a lower frequency, f_l, by projecting a known pattern on the sample (structured illumination). A beat low-frequency pattern will now appear on the superposition area of the illuminating pattern and the finely detailed sample, both of them of high frequency, as illustrated in Fig. 6. This effect is called moiré; it contains information on the spatial frequency of the two superimposed high-frequency patterns, and if the features of the illumination pattern are known, then the unknown pattern (the sample structure) can be recovered from the moiré fringes, which are of lower frequency and will have been efficiently detected. Such an imaging process, which requires 15 different illumination patterns, renders images with a higher-frequency content resulting in finer detail and, consequently, increased resolution. Resolution is increased in this manner by a factor of 2 (≈120 nm laterally) [99], and it can be extended to imaging multiple and simultaneous fluorophores [100]. Remarkably, SIM at this resolution does not require special fluorescent probes.

Nonlinear saturation of molecular transitions was proposed to further increase the resolution with no theoretical limit (nonlinear SIM or saturated SIM, SSIM) [101, 102], but the high light intensities required to saturate the excited state of standard chromophores are not compatible with biological imaging. Reversible photoswitching of a fluorescent protein provides the required nonlinear response at light intensities six orders of magnitude lower and has very recently been shown to be a biologically compatible super-resolution imaging method, achieving a resolution of 50 nm in TIRF configuration [103]. SSIM acquisition only comprises 25 images at moderate intensities on the order of 1–10 W cm^{-2} and has, thus, great potential for live-cell imaging.

[1] Please note that structured illumination microscopy is also commonly used to designate a diffraction-limited optical sectioning methodology based on patterned illumination [98].

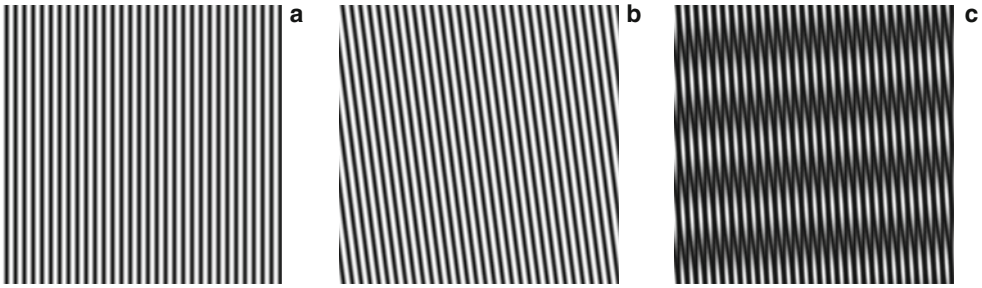

Fig. 6 SIM working principle: An image can be described as the sum of spatially varying patterns of different frequency: High spatial frequencies are associated with steep intensity variations on the image, such as highly detailed structures, whereas low frequencies correspond to smooth variations in the intensity, such as a background. The maximal resolution that can be attained is limited by the highest frequency that can be relayed through the objective lens; hence, details on the sample corresponding to very high spatial frequencies are lost. High-frequency components, f_h, can be, however, offset to a lower frequency, f_l, that is efficiently imaged through the objective lens. This is the basis of SIM: the projection of a known pattern (structured illumination, **a**) on an unknown high-frequency pattern, f_h (the sample, **b**), results in a pattern of lower frequency, f_l (dark stripes on **c**), from which the unknown pattern can be recovered: $f_h = f_l + \Delta f$, where Δf is the frequency offset between the dark stripes on **c** and the known illumination pattern on **a**

3D SIM. Temporal resolution and live-cell imaging

3D SIM was demonstrated several years ago [104], but the need for mechanically swapping 15 patterns per optical section slowed down the whole process turning 3D imaging cumbersome and impractical. After replacing the optomechanics for a spatial light modulator, 3D SIM has been demonstrated on living cells with low light intensities of ($\approx$5 W cm^{-2}), requiring only about 5 to 25 s per complete cell [105]. Spatial resolution was twice that of conventional microscopy, and temporal resolution was only limited by the CCD read-out time. A simpler experimental realisation has been recently reported (multifocal SIM) [106].

Probes and labelling systems

The spectroscopic properties of the chromophores are determinant for achieving maximal resolution, as subdiffraction imaging conditions are much more stringent than those of widefield or confocal microscopy.

Fluorescent probes for STED imaging

During STED imaging, fluorophores undergo excitation followed by depletion by a high-intensity red-shifted beam. The fluorophore must have a high quantum yield and large absorption cross section at the excitation wavelength and also a large stimulated-emission cross section but negligible excitation cross section at the depletion wavelength. This last requirement is important as further electronic promotion of the molecule from an excited state (either singlet or triplet) through absorption of a depletion beam photon would result in intolerable bleaching and reduced stimulated emission rate. So far, more than 40 different fluorophores covering almost entirely the visible spectrum have been used in STED imaging.

Fluorophores used for STED imaging may either be small organic dyes covalently coupled to antibodies, genetically encoded fluorescent proteins or genetically encoded tags that selectively bind small molecules. Immunolabelling is currently the most popular approach to STED imaging. It allows labelling of structures in fixed and permeabilised cells with a broad library of dyes mainly belonging to the Atto family and also some Alexas and Coumarines that span from the blue edge of the spectrum to the red (e.g. Atto390, Atto532, Atto565, Atto647N [10, 14, 107–111]).

Specific targeting with fluorophores is, however, essential for tackling biological problems. STED imaging can be performed on fusion constructs of fluorescent proteins that also span most of the visible spectrum: green (GFP [112]), yellow (YFP [113] and citrine [114]) and far-red emitting proteins (TagRFP657 [115] and the tetrametric E2-Crimson [116]). Several reversible photoswitchable proteins have also been demonstrated suitable for RESOLFT imaging, exploiting their reversible switching behaviour to deplete the periphery of the focal spot (Dronpa and its counterpart Padron derivative [15, 22], rsEGFP2 [23] and Dreiklang [117]).

A further approach that also targets the fluorophores to cellular components is based on genetically encoded polypeptide tags that can be fused to the protein of interest and specifically bind synthetic fluorophores that are permeable to the membrane. The main advantage of these self-labelling systems is that they can be used with organic fluorophores that are smaller and more photostable than FPs; the drawback is that most of the fluorophores suited for STED are not membrane-permeable. One of the systems that have been used for STED imaging on living cells is based on the modified enzyme haloalkane dehalogenase (HaloTag [118]) [119]. Similarly the SNAP and CLIP tags [120, 121] based on the human DNA repair protein O^6-alkylguanine-DNA alkyltransferase have too allowed STED imaging on living cells [122]. As SNAP and

CLIP fusion proteins can be labelled simultaneously and specifically with different molecular probes, dual-colour STED imaging of living cells is also possible [29].

Fluorescent probes for localisation microscopy

Localisation microscopy needs fluorophores that are controllably converted between a fluorescent active (ON) state and a nonfluorescent inactive (OFF) state or between different colours, either spontaneously or upon irradiation with light. Fluorophores must be bright and show a high contrast between both states as every photon emitted from a fluorophore in an OFF state will contribute to the background degrading localisation precision. Most of the times conversion between one state and the other is induced by light, and hence, fluorophores are termed photoconvertible.

An important feature of the probes used for stochastic LM imaging is that their switching rate constant r, defined as the ratio of the average time the molecule spends in the ON state (τ_{On}) to the average time it spends in the OFF state (τ_{Off}), $r=\tau_{On}/\tau_{Off}$, determines the resolution that can be achieved. A densely labelled structure may contain N_{Total} number of fluorophores in a diffraction-limited region (roughly 1,000 in a planar configuration). In the most common PALM/STORM implementation, only one molecule per diffraction-limited region can be unequivocally identified and localised; thus, in order to keep that one single molecule in its active state while the rest are inactive, the lifetime of the OFF state must be at least N_{Total} times longer than the lifetime of the active state: $\tau_{Off}>N_{Total}\times\tau_{On}$ ($\tau_{Off}>1{,}000\times\tau_{On}$ in our example). This guarantees that only a sparse subset of molecules will be active at any time during the acquisition process and, in turn, defines the trade-off between spatial resolution, limited by the labelling density, and the temporal resolution of the experiment. The switching rate can be tuned through control of the activation and excitation lasers and the concentration of an oxidising agent (see below).

In general, photoconvertible fluorophores can be either photoactivatable, photochromic or photoswitchable: photoactivatable, if they are irreversibly switched from a dark to a bright state; photochromic, if they change colour upon irradiation; or photoswitchable, if they can be reversibly switched from a dark to a bright state. They can be either genetically encoded (PALM and FPALM) or synthetic organic fluorophores (STORM or *d*STORM). For the sake of nomenclature, it is worth noting that, whichever nature of the conversion mechanism, photoconvertible fluorescent proteins are very often termed in literature with the acronym PA-FPs. There are prominent differences that result from the use of photoconvertible fluorescent proteins or synthetic organic fluorophores: PA-FPs have maximal labelling efficiency and specificity, and they are smaller (the barrel in which the FP chromophore sits is 2.4×4.2 nm [123], while the size of an IgG antibody is ≈7–8 nm); on the contrary, synthetic fluorophores show higher photostability and brightness than PA-FPs, which results in higher localisation precision, and their photoswitching rates can be controlled by external means, which allows faster acquisitions. Both types of fluorophores may be used for imaging living cells; in the case of synthetic fluorophores, appropriate labelling systems and reducing conditions are required [124, 125].

Photoconvertible fluorescent proteins More than 20 photoconvertible fluorescent probes have been reported (see Table 2) including photoactivatable, photochromic and photoswitchable FPs. Some of them are bright but tetrameric, which hinders their use in biological problems. Dronpa (switches from dark to bright [139]) and mEos2 (converts from green to red [133]) are currently the photoconvertible proteins of choice for most biological applications because they show a high contrast between fluorescent states and they are monomeric (although there have been reports on the non-monomeric nature of mEos2 [134]). PS-CFP2 (converts from cyan to green [137]) and PSmOrange (converts from orange to red [138]) also show good spectroscopic properties and may be used to simultaneously tag two intracellular proteins. PAmKate is the farthest red-shifted photoactivatable protein [128], which facilitated multicolour PALM of cells simultaneously expressing Dendra2, PAmCherry1 and PAmKate-tagged proteins with a single excitation wavelength [128].

The exact mechanisms involving photoconversion are still unclear in many cases. Photoactivation may involve a one-step photoinduced transition from the dark neutral form of the chromophore to a brightly fluorescent anionic form (e.g. PA-GFP [143]) or a two-step photooxidation that induces backbone cyclation and ensuing formation of the chromophore (e.g. PATagRFP [130]). Photochromatism usually involves a two-step photooxidation process that causes cleavage of the polypeptide backbone (e.g. PSmOrange and EosFP [138, 144]). Photoswitching involves *cis–trans* isomerisation of the chromophore accompanied by a change of its protonation state (the anionic state being the fluorescent state and the protonated the nonfluorescent—interestingly, the chromophore can be fluorescent in both the *cis* and the *trans* conformations as long as the protein scaffold keeps it in a planar conformation) [145–147]. When kept in the dark, these proteins relax to the thermodynamically stable *cis* conformation within minutes to several hours; in thermal equilibrium, the photoswitchable proteins predominately populate the *cis* conformation with the chromophore in the anionic state.

Synthetic probes for localisation microscopy (STORM) The fundamental mechanism of switching synthetic dyes is the formation of a nonfluorescent anionic state through

Table 2 Commonly used monomeric photoconvertible fluorescent proteins

Protein	Excitation (nm)	Emission (nm)	Ext. coeff (10^3 M^{-1} cm^{-1})	φ_{Fl}	Reference
Photoactivatable proteins (from dark to bright)					
PA-GFP	504	517	17.4	0.8	[126]
PAmCherry2	570	596	24	0.53	[127]
PAmKate	586	628	46	0.66	[128]
PAmRFP1	578	605	10	0.08	[129]
PATagRFP	562	592	66	0.38	[130]
Photochromic proteins (from one colour to another)					
Dendra2 (green)	486	558	45	0.50	[131]
Dendra2 (red)	505	575	35	0.55	
mClavGR2 (green)	488	504	19	0.77	[132]
mClavGR2 (red)	566	583	32	0.54	
mEos2[a] (green)	506	519	56	0.84	[133]
mEos2 (red)	573	584	46	0.66	
mEos3.2 (green)	507	516	0.84	63.4	[134]
mEos3.2 (red)	572	580	0.55	32.2	
mKikGR (green)	505	515	0.69	49	[135]
mKikGR (red)	580	591	0.49	28	
mMaple (green)	489	505	15	0.74	[136]
mMaple (red)	566	583	30	0.56	
PS-CFP2 (cyan)	402	468	34	0.6	[137]
PS-CFP2 (green)	490	511	27	0.19	
PSmOrange (orange)	548	565	113.3	0.51	[138]
PSmOrange (red)	634	662	32.7	0.28	
Photoswitchable proteins (reversible switching from dark to bright)					
Dreiklang[b]	511	529	83	0.41	[117]
Dronpa	503	518	95	0.85	[139]
mGeos-M	503	515	51	0.85	[140]
Padron[c]	396	522	43	0.64	[48]
rsCherry	572	610	(80)	(0.02)[d]	[141]
rsFastlime	496	518	39	0.77	[142]
rsEGFP2	478	503	61.3	0.3	[23]

φ_{Fl} the fluorescence quantum yield

[a]mEos2 is thought to be monomeric but a tetrameric structure has been recently reported [134]

[b]Dreiklang's fluorescence is disentangled from switching: It is activated at 340 nm and deactivated at 412 nm [117]

[c]Padron's switching behaviour is Dronpa's reversed (hence the name): Irradiation with blue light (503 nm) transfers the protein chromophore from the OFF to the ON state and concurrently induces fluorescence; irradiation with UV light switches this photoswitchable protein back to the OFF state

[d]From [127]

photoreduction of the triplet state of the chromophore in the presence of thiols in aqueous solvents; this anionic state is nonabsorbing at the excitation wavelength and survives in the presence of molecular oxygen for several milliseconds to hours. Upon oxidation by molecular oxygen, the chromophore returns to the singlet ground state, and hence, fluorescence is recovered [38]. Both processes are facilitated on irradiation: Excitation of the fluorophore pumps the molecule into the triplet state, which can now be reduced by thiols, and direct excitation of this anionic intermediate state (most anionic states are absorbing at ≈405 nm) facilitates recovery of the fluorescent form. It is worth noting that a fluorophore in its neutral (non-reduced) triplet state is sensitive to irreversible photobleaching through photoionisation and reaction with molecular oxygen, which in turn results in production of reactive oxygen species (one of the major sources of phototoxicity in the cell in conventional microscopy). However, the formation of a reduced triplet state favoured in localisation microscopy protects the fluorophore from photobleaching.

Adequate control of the concentration of reducing and oxidising agents allows the photoswitching rate of the chromophore to be tuned: The average time the fluorophore spends in the ON state, τ_{On}, is controlled through the excitation power and the concentration of thiols; the average time in the OFF state, τ_{Off}, is controlled through the anion excitation intensity (usually at ≈405 nm) and the concentration of molecular oxygen. As the photoswitching rate of the chromophore determines the density of active fluorophores and, in turn, the spatial and temporal resolution of the experiment

(see above), STORM imaging of cellular structures with different labelling density can this way be optimised.

Many green, red and NIR-emitting standard fluorophores (e.g. most carbocyanines, Alexa and Atto dyes [37, 38, 148, 149]) can undergo switching. A recent report has evaluated 26 synthetic fluorophores on the basis of the emitted photons per switching event, on-off duty cycle, photostability and number of switching events, identifying as best-performing dyes for STORM imaging Atto488 for the blue spectral window, Cy3B for the yellow window, Alexa 647, Cy5 and Dyomics 654 for the red and DyLight 750, Cy7 and Alexa 750 for the NIR window [150]. The choice of red-ox buffer composition is another important factor in achieving robust imaging [150]: Suitable reducing agents are β-mercaptoethanol or mercaptoethylamine and glutathione [37]—this latter is endogenous and, hence, enables live-cell STORM.

Similar to live-cell STED, live-cell STORM also requires the use of genetically encoded polypeptide tags: trimethoprim conjugates [124], HaloTag [151], SNAP-Tag [125] or tagging with small tetracysteine motifs and the fluorescein arsenical helix binder FlAsH [152, 153]. Photoswitchable proteins and genetically encoded tags can be expressed simultaneously in the same cell: A recent combination of HaloTag labelling (Atto655) and expression of PATagRFP and PA-GFP has allowed triple colour STORM/PALM imaging in living cells [154]. It should be highlighted that these small motifs, which are encoded by less than ten amino acids, may be particularly convenient for labelling proteins that do not tolerate large protein fusions.

Spatial resolution. Resolution vs. localisation accuracy

Early reports on stochastic LM stressed the achieved localisation precision as it was commonly assumed that localisation statistics for single emitters set the resolution of the image. However, the localisation precision of 20 to 30 nm for a single molecule is not directly translated into actual structural resolution as fine details of the specimen cannot be discerned if labelling is too sparse, as illustrated in Fig. 5d, e: undersampling or insufficient labelling results in artefactual discontinuous structures. Accurate description of a biological structure requires that the mean distance between localised neighbouring molecules be at least twice as fine as the desired resolution (Nyquist–Shannon theorem [155]). Ram et al. [156] proposed a resolution measure which gives a bound for the accuracy with which the distance between two point sources can be estimated taking into account photon statistics, pixelation of the detector and other resolution-degrading experimental factors, yet it does not incorporate the labelling density. Another interesting resolution measure was proposed by the Schnitzer group considering a feature of the specimen resolvable when a microscopist can reliably estimate it from the data: This measure incorporates the precision of emitter localisation, labelling density and prior information regarding statistical properties of the object and the imaging system [157, 158].

Quantitative super-resolution

Subdiffraction images contain a vast amount of information organised in complex spatial and temporal patterns that often resemble an apparently random distribution of unrelated coloured dots. Researchers have become increasingly aware of the need for statistical tools to analyse the spatial correlation between molecules and clusters of molecules and quantitatively describe the organisation of proteins at the nanoscale. Ideally, an analytical method for quantifying super-resolution images would evaluate the spatial distribution of the detected molecules to provide an assessment of their number, their aggregation state, the size of the aggregates and their density.

Ripley's K-function quantifies clustering as a function of length scale [159]. The analysis determines the sizes and shapes of protein clusters by comparing the distributions of individual molecules or clusters of molecules located inside concentric circles of increasing diameter centred on each localised event to what would be expected from a random distribution:

$$L(r) = \sqrt{\frac{N(r)}{\pi\rho}} \tag{4}$$

where $N(r)$ is the observed number of molecules within radius r and ρ is the average number of molecules per unit area. $L(r)$ is actually the normalised Ripley's K-function: If molecules are randomly distributed, $N(r) = \pi\rho r^2$ and $L(r) = r$ (within a certain uncertainty); in the case of a clustered distribution, $L(r) > r$. The maximum of the normalised K-function is a measure of cluster size and lies between the radius and the diameter of the cluster, yet also depends on the distance between individual clusters [160]. Its value approaches the diameter of an individual cluster at large inter-cluster distances.

A drawback of the application of Ripley's K-function analysis to PALM or STORM data is that almost all fluorophores exhibit inherent blinking: Once activated, a PA-FP reversibly switches between a fluorescent and a nonfluorescent state on timescales ranging between microseconds to seconds before converting to an irreversible dark state [161, 162]. In this case, Ripley's K-function is subject to over-counting. An alternative way to quantitatively characterise super-resolution PALM/STORM images that is not much affected by multiple appearances of a single molecule at distances larger than the PSF is pair-correlation function analysis [163–165]. The

pair-correlation function $g(r)$ measures the probability of finding another protein at a distance r compared to that expected from a random distribution of proteins. If the proteins are not randomly organised, $g(r)>1$; if the distribution of proteins is random, $g(r)\approx 1$. A blinking fluorescent protein or a photoswitchable one that has been repeatedly photoactivated will appear several times in a region defined by the width of the PSF (hence, $g(r)>1$ for distances r smaller than the width of the PSF) but will not be correlated with proteins at larger distances. A recent work has demonstrated the utility of pair-correlation function analysis for characterisation of membrane heterogeneity [166].

Nanoscopy applications

Despite its short history, fluorescence nanoscopy has been rapidly adopted in many areas of biology. Among them, the areas that are undergoing a significant transformation from the insights obtained at the nanoscale are those that involve ensembles of molecules that either assembly to form large-scale complex cellular structures or interact in response to signalling events. It is not possible to discuss all the applications of light nanoscopy; instead, prominent examples on reports that have studied cellular structures, membrane organisation, dynamic assembly of proteins, neurobiology and virology are presented. Applications of nanoscopy to the study of membrane organisation and neurobiology stand out as they are driving promising developments on quantitative data analysis, fluorescent probes and experimental design. It is worth noting that fluorescence nanoscopy is still under development, and thus, many reports on the application of super-resolution techniques concern proof of concept.

Cellular structure

Cellular ultrastructure has been traditionally studied with electron microscopy (EM), a technique that has exquisite spatial resolution, yet is unable to resolve dynamics and may induce structural perturbations due to complex sample preparation procedures. Whereas EM yields better-resolved structures, optical nanoscopy benefits from the specificity of fluorescent tagging and live-cell imaging capabilities at molecular resolution. Correlative light nanoscopy and EM [167, 168] or atomic force microscopy [169] are being used to complement and validate subdiffraction images, giving an anatomical context that enriches data interpretation.

Cell architecture (description and dynamics)

Combining astigmatic 3D STORM imaging and dual-objective detection (see above, "Stochastic localisation microscopy in 3D" section), the Zhuang group has achieved imaging at a resolution below 10 nm in the lateral direction and 20 nm in the axial direction [32]. Such an impressive resolution allowed them to observe the 3D ultrastructure of the actin cytoskeleton, revealing two layers of continuous actin networks with distinct structures in sheet-like cell protrusions. Another dual objective arrangement (iPALM) allowed observation of the 3D nanoscale protein organisation of integrin-based cell adhesions at 20 nm lateral resolution and 15 nm axially. It was found that integrins and actin are vertically separated by a ≈40-nm focal adhesion core region consisting of multiple, partially overlapping, protein-specific strata, including a membrane signalling layer, an intermediate force transduction layer and an uppermost actin-regulatory layer [170].

Optical super-resolution is also able to follow dynamic remodelling of cellular architecture. The dynamic nano-organisation of integrins and talin inside focal adhesions has recently been studied: direct visualisation of integrin and talin movements demonstrated that focal adhesions are specialised platforms priming integrin immobilisation and revealed nanopartitioning within the focal adhesions that defines the precise location and duration of integrin-specific biochemical and mechanical signals [171].

Organelle delineation and topography

The endoplasmic reticulum (ER) was one of the first organelles targeted by STED imaging: The fluorescent protein citrine concentrated on the ER permitting volumetric imaging of this organelle [114]. The Zhuang lab has also very recently demonstrated super-resolution STORM imaging with membrane probes, such as carbocyanine dyes with alkyl chains (DiI, DiD, DiR), cationic dyes (MitoTracker) and BODIPY conjugated probes (Er/LysoTracker) specific to the plasma membrane, mitochondria and ER or lysosomes, respectively, capturing details of morphological dynamics of mitochondrial fusion and fission and ER remodelling [172]. The cell permeability, small size and high affinity of these probes facilitated targeted high-density labelling of organelles in live cells, improving resolution as a result. However, when imaging at high resolution using these probes, caution has to be taken as artefacts may arise from phototoxicity: in particular, the mitochondria showed stress symptoms after imaging for 1 min. With the same aim of increasing labelling density to improve resolution, the same group (in collaboration) proposed a method to label neuron membranes at high density and demonstrated that, compared to cytoplasmic labelling, high labelling density of neuron membranes significantly improved neuron tracing accuracy [173].

Mitochondria

The distribution of proteins in the mitochondria has been the focus of several studies using optical nanoscopy. More

methodologically oriented than biologically driven, one of the earliest demonstrations of *d*STORM targeted intracellular FoF1-ATP synthase and cytochrome c oxidase in the inner membrane of the mitochondria in fixed cells, showing that it was possible to draw quantitative conclusions from the distribution of proteins [174]. In a tour de force to unravel the distribution of the translocase of the mitochondrial outer membrane (TOM) complexes in the outer membrane, the Jakobs lab STED-imaged more than 1,000 fixed cells. They determined quantitatively the nanoscale distribution of Tom20 (a subunit of the TOM complex) and concluded that TOM complexes aggregate in clusters with a density finely adjusted to the cellular growth conditions and the distribution of the cell within a microcolony [175]. The nanoscale organisation of TOM complexes has also been studied in live cells through localisation of Tom20 and ATP synthase [176].

Nucleus

The vertebrate nuclear pore complex (NPC) is a ≈120-MD protein complex that mediates communication and selective exchange between the nucleoplasm and the cytoplasm. Its structure has traditionally been analysed by electron microscopy, but this technique cannot provide specific labelling of the molecular components. The complexity of sample preparation procedures for light nanoscopy and the need for refined image analysis evidence that imaging the structure of the NPC is particularly challenging.

The structure of NPCs in isolated *Xenopus laevis* oocyte nuclear envelopes was investigated at a lateral resolution of ≈15 nm using *d*STORM with two bright fluorophores (Atto520 and Alexa 647). Taking advantage of the self-similarity of NPCs, the authors accumulated several hundreds of super-resolved images of NPCs that allowed them to determine the diameter of the central NPC channel (41 ± 7nm) and to demonstrate that the integral membrane protein gp210 is distributed in an eightfold radial symmetry [177].

Dual-colour PALM was used to study the subnuclear distributions of general transcription factors TFIID and TAF3 [178]: The Tjian group reported differential subnuclear distributions of transcriptions factors TAF3 and TFIID relative to the nuclear periphery, where the key myogenic gene *MyoD* is preferentially localised in myoblasts and suggested that intranuclear sequestration of core target components and their target genes provides an additional mechanism for promoter selectivity. It is worth noting the complexity of imaging individual transcription factor molecules in the context of nuclear architecture: Cells had to be grown on sapphire disks, high-pressure frozen, freeze substituted, embedded in a resin for polymerisation and finally mechanically cut in 100 nm sections that had to be kept in the dark before imaging.

Chromosome organisation

Direct super-resolution imaging of chromosomal DNA is still hindered by the lack of compatible labels. Fluorescently tagged histones have been used to infer structural features at the nuclear nanoscale in fixed cells [179] and to investigate nucleosome and chromatin movement in living cells [124], but, due to the nature of histones, the achieved density of labelled chromatin is low. Taking advantage of the compatibility of SIM with standard fluorophores, 3D-SIM permitted higher-order chromatin structure and the relative localisation of NPCs and nuclear lamina at the nuclear periphery to be probed in mammalian cells at ≈100 nm resolution using DAPI, a dye which directly binds DNA, and NPC- and lamin b-specific antibodies [100]. Stochastic LM imaging on isolated DNA has been demonstrated using DNA intercalating dyes [180, 181], but this methodology still needs to be refined in order to be used in whole cells [182]. Recently, the Heilemann lab has reported on a click chemistry reaction for DNA labelling that allowed bright photoswitchable carbocyanine (Alexa 647) fluorophores to be introduced into DNA at a density compatible with *d*STORM imaging at 20 nm resolution [183]. Chromosomal organisation in bacteria using super-resolution imaging has been studied with nucleoid-associated tagged proteins (HU, H-NS), revealing their distribution in clusters at different stages of the cell cycle [184] and hinting at a key role in global chromosomal organisation [185].

Quantitative description of the molecular organisation at the plasma membrane

The organisation of lipids and proteins in membranes has been the subject of investigation of biophysicists and biochemists for decades, but diffraction-limited fluorescence microscopy lacks the spatial resolution required to resolve the dynamic molecular associations that take place in the membrane. Stochastic LM and STED-based imaging allow visualisation of structures at the same scale at which protein clusters and lipid domains are postulated to exist. In particular, multicolour LM measurements allow spatial correlations between individually identified proteins that belong to different classes to be quantified at the single molecule level.

The interplay between protein–protein and protein–lipid interactions in determining clustering properties is still under debate. Ripley's K-function analysis of dual-colour PALM imaging of the membrane anchors of Lck and Src, demonstrated that membrane proteins can cluster together or be excluded from each other based solely on their membrane targeting sequences [186]. Pair-correlation analysis of PALM images has revealed distinct nanoscale organisation of two plasma-membrane proteins with different membrane anchoring and lipid partitioning characteristics (the inner leaflet lipid-anchored protein Lyn and the transmembrane protein Lat)

and PA-GFP tagged to glycophosphatidylinositol (GPI), an outer leaflet protein arrangement, in COS-7 cells. All three proteins were found to reside in clusters of different size and molecular densities, possibly indicating that it is a combination of the specific membrane targeting sequence and lipid composition that modulates the distribution of proteins. Cross-correlation analysis of actin and PA-GFP-GPI protein arrangements showed cluster co-localisation upon cross-linking of GPI, suggesting that the actin cytoskeleton is involved in protein reorganisation and cluster stability [166]. Also, acetylcholine receptor in the membrane of Chinese hamster ovary (CHO) cells was shown to aggregate in clusters of ≈55 nm. Ripleys's K-test on STED images revealed changes in the nanocluster distribution at the nano- and micrometre scale upon cholesterol depletion, indicating that besides cholesterol and saturated lipids, proteins (especially those related to the cytoskeleton) play an important role in membrane organisation [187].

PALM imaging of living cells has given evidence that there is a direct link between the actin skeleton and the organisation of proteins in domains at the membrane. In the first application of PALM to living cells, the Hess group showed that influenza hemagglutinin (HA), a protein associated with cholesterol-rich membrane domains, resides in irregular clusters on length scales from few nm up to many micrometres; furthermore, these observations discarded the hypothesis that line tension (due to lipid fluid-fluid phase coexistence) is responsible for the shape of the domains [188]. PALM imaging of live fibroblasts has also demonstrated that both transferrin receptor (TfR) and HA are correlated with actin while TfR and HA are uncorrelated, providing with the first direct evidence that TfR and HA live in distinctly different domains and also suggesting a direct interaction of membrane proteins with the actin skeleton [128].

Super-resolution has revealed that protein organisation patterns are dependent on the cell type: Systematic comparison (PALM) of the β-2 adrenergic receptor with a nonclustering small peptide has been another recent methodological approach that has shown that this protein is associated in nanosized clusters only in cardiomyocytes such as H9C2 cells, but not in other cell lines, such as HeLa or CHO. The authors found that clustering was influenced by the actin cytoskeleton, but it was not affected by cholesterol removal, thus ruling out the possibility that clustering of β-2 adrenergic receptor is dependent on lipid phase [189].

The role for cholesterol and saturated sphingolipids in membrane organisation is far from understood yet. The combination of STED and FCS has allowed the study of the nanoscale dynamics of membrane lipids in a cell, showing that sphingolipids were transiently trapped in cholesterol-mediated molecular complexes of sizes below 20 nm, whereas phosphoglycerolipids were not [18]. STED-FCS has also revealed a lipid–protein transient bonding that is dependent on the interacting species and is different from that responsible for forming cholesterol-dependent, liquid-ordered domains in model membranes [20]. PALM-suitable probes based on lipid-binding domains of theta-toxin and lysenin, which bind to cholesterol and sphingomyelin membranes, respectively, have been designed with the aim of directly imaging structural components of membrane domains with single molecule sensitivity. PALM imaging of these probes showed that cholesterol and sphingomyelin-enriched domains have different shapes and occupy different regions on the plasma membrane [190]. Using a PAINT methodology with Merocyanine 540, a probe whose fluorescence is sensitive to the lipid phase, it has been possible to tell liquid- and gel-phase nanoscale domains in binary lipid bilayers [191].

The nanoscale organisation of Syntaxin1 has been frequently addressed: It was one of the first proteins to be directly observed in clusters which exhibited a diameter of 50 to 60 nm in PC12 cells and were not dependent on the lipid phase [110, 192]; a recent work showed that syntaxin clustering is mediated by electrostatic interactions with strongly anionic lipids (PIP2), and so protein–lipid interactions can result in the formation of microdomains independently of cholesterol or lipid phases [193]. In a recent demonstration of the need for more powerful analytical tools, a quantitative cluster analysis of nanosized syntaxin clusters in PC12 cells showed that the density of the molecules gradually decreases from the dense cluster core to the periphery. It was also showed that syntaxin and SNAP-25 clusters are morphologically different [194].

Signalling. Dynamic assembly of proteins

The application of super-resolution imaging techniques to the study of signalling events is closely related to the study of heterogeneity at the plasma membrane. Upon a signalling event, the dynamic assembly (spatiotemporal sequence) of effector molecules at the plasma membrane initiates a signalling cascade that regulates cellular activity. Diffraction-limited microscopy has been widely applied to the study of signalling events yielding valuable information on the cellular distribution of signalling components, whereas super-resolution microscopy has permitted recognition of protein islands, description of signalling microclusters and determination of the stoichiometry of molecule assemblies.

Determination of the photophysical rate constants of two photoswitchable fluorescent proteins (Dronpa and tdEos) allowed the Baumgart group optimisation of dual-colour PALM imaging, which, in turned, permitted quantitative analysis of the spatial correlation between kinase ZAP70 and adaptor SLP76 microclusters on the periphery of T cells and of the effects of F-actin on microcluster assembly upon recognition of antigens by T cell receptors [195]. They found that, upon T cell activation, the average radii of SLP76 and Lat microclusters decreased whereas ZAP70

microclusters remained constant and that their morphology is affected by actin polymerisation.

Using PALM and FCS, the Davis group followed the behaviour of TCR (T cell antigen receptor) and Lat islands during T cell activation: They found that TCR and Lat are expressed on separate protein islands on T cell membranes and concatenate during activation giving rise to TCR and Lat microclusters. Curiously, the individual islands within the microclusters remained intact, and intermingling of TCR and Lat molecules did not occur [196]. An explanation to this result also came from PALM experiments: The Gaus group visualised Lat clusters growing in fluorescence intensity and then fading, which is characteristic of species localised in vesicles. This way the authors showed that TCR signalling depends on Lat molecules that are associated with intracellular vesicles, rather than pre-existing clusters of Lat molecules at the plasma membrane. These observations helped determine that it is vesicular Lat and not plasma-membrane-bound Lat which makes the bulk contribution to signalling [197].

Two-colour SIM on fixed natural killer (NK) cells has revealed the organisation of actin cytoskeleton at the NK cell synapse. The cytotoxic function of NK cells is regulated through rearrangement of receptors, signalling molecules and cytoskeleton at the immune synapse. The Davis lab defined the cortical actin structure within the central region of the NK immune synapse and demonstrated that synaptic remodelling of the F-actin mesh occurs at this central region [198].

Neurobiology

While it is possible to identify synaptic spines by conventional microscopy, axons and important structural and functional domains of synapses are too small to be properly resolved on diffraction-limited images. Characterisation of the synaptic ultrastructure has, thus, primarily relied on EM, but EM is not applicable to living cells. The nanoscale distribution and dynamics of synaptic proteins is, therefore, essentially unexplored.

Fluorescence nanoscopy makes possible the investigation of the nanoscale dynamic organisation of proteins within subsynaptic domains: The fate of synaptic vesicles after exocytosis and fusion with the membrane has been studied by STED microscopy in fixed [199, 200] and live neurons using video-rate (20–28 Hz) [27, 201] and time-lapse STED microscopy [202, 203]. AMPA receptors trafficking in neuronal cells have been investigated by single particle tracking PALM [204]. This approach was also used to study the dynamics of individual actin molecules in spines of live cultured neurons [85] as well as the morphological changes of dendritic spines cytoskeleton in response to induced synaptic activity over 30 min [205]. The strategy for successful long-term localisation without irreversibly bleaching the fluorophores was to use a photoswitchable protein (tdEos) fused to a low affinity actin-binding peptide that allowed replenishment of the fluorophore.

Beyond cultured cells, the nanoscale distribution of ten pre- and post-synaptic proteins components has been characterised in fixed mouse brain sections using multicolour 3D STORM, showing that there is an orderly alignment of proteins and receptors along the longitudinal axis of the synapse [206]. Super-resolution of fixed brain sections is also feasible: The morphological plasticity of dendritic spines in living brain slices has been described using YFP as a volume label with time-lapse STED microscopy [113].

STED imaging of living organotypic brain slices of Lifeact-YFP, a small peptide that binds actin with low affinity [207], revealed that the width of spine necks is dynamic and changes in response to the induction of chemical long-term potentiation [208]. Going one step farther, STED has been demonstrated on the living brain of an anaesthetised mouse expressing YFP as a nonfusion protein in the neuronal cytoplasm [28]. The high average power required for STED imaging hinders, however, its application to live tissue. Recently, RESOLFT imaging of photoswitchable proteins, which takes advantage of the lower power required to drive the fluorophore from the active to the inactive form and back, has been demonstrated on living organotypic hippocampal slices that had been transfected with Lifeact-Dronpa [24].

HIV

Viral assembly is widely studied using HIV-Gag, the main structural protein of HIV. This protein has received much attention since the early proof-of-concept reports of super-resolution, studying the assembly and dynamics of tdEos-Gag [34, 41]. Gag clusters have been imaged at subdiffraction resolution to quantitatively characterise their size and morphological characteristics in different stages of their formation [209]. Importantly, the authors also found that fusion proteins Gag-mEos and Gag-tdEos organised differently, confirming previous evidence that fluorescent proteins (or at least large ones as tdEos) interfere with the assembly [210]. The Piguet group established fluorescence labelling of Gag and tetherin, concluding that mEos and Dronpa constructs had minimal impact on infectivity and used multicolour PALM and quantitative cluster analysis to investigate the mechanism of tetherin-mediated HIV restriction [210]. The distribution of the HIV-1 Gag protein on the plasma membrane of virus producing cells has also been studied revealing three patterns of organisation: patchy aggregation of Gag proteins, organisation in small dense clusters and organisation in ≈140-nm-sized clusters consistent with a 3D hemispherical assembly that are suggested to correspond to viral assembly sites [211].

Viral assembly has been studied at nanoscale resolution (≈40 nm) STED imaging the viral envelope glycoprotein

distribution on individual HIV-1 particles using fluorescently tagged antibodies that recognised viral envelope surface glycoprotein gp120. Correlation of the viral envelope surface clustering with the viral entry efficiency revealed that clustering the envelope surface into a single focus is of particular importance for efficient HIV-1 entry and that rearrangement of the inner protein lattice is coupled to alteration of the virus surface in preparation for entry [212].

The integrase enzyme of HIV-1 is another protein that is also disrupted by fusion to fluorescent proteins. The Zimmer group first established that FlAsH tagging [152] preserved its biological function and proceeded to demonstrate PALM imaging of proteins tagged with small tetracysteine motifs and the fluorescein arsenical helix binder (FlAsH-PALM), allowing successful nanoscopy of the integrase enzyme of HIV-1 in host fixed and living cells under conditions that fully preserved HIV-1 infectivity. This way they showed that an important fraction of the cytoplasmic viral material remains encapsidated and that capsids can be found in the cytoplasm [153].

Outlook

Fluorescence nanoscopy has already left the physics lab and specialised microscopy conferences and has become available as a new addition to the methodological toolbox. Major microscope manufacturers have commercialised user-friendly instruments, and many labs have developed their own home-made super-resolution microscopes.

Fluorescence nanoscopy is, nevertheless, still under development. Progress hinges heavily on the availability of new probes with refined spectroscopic behaviour and also on experimental designs that address current instrumental constraints, but many fundamental insights will remain inaccessible if data analysis methods do not uncover the wealth of information hidden in images with macromolecular resolution.

Extraction of information beyond structure still represents a challenge: Quantitative analysis of the molecular organisation patterns that are observed at subdiffraction resolution will provide a starting point for functional interpretation of molecular clustering, yet there is a need for statistical tools that better characterise their complexity. More accurate and reliable description of the molecular patterns will require a better understanding and a tighter control of the photophysical behaviour of the fluorescent probes.

Resolution needs to be improved beyond the current 20 to 40 nm and towards isotropic 3D resolution. Systematic errors such as sample drift and camera irregularities will need to be compensated, the effect of molecular orientations on resolution will have to be taken into account and algorithms will have to deal with the presence of a large background. It will also involve the development of fluorophores that can deliver more photons before bleaching. Also, red-shifted fluorescent probes will be advantageous as cellular autofluorescence is the source of an unwanted background that reduces contrast and degrades resolution. Smaller probes and labelling systems will be demanded (e.g. nanobodies [213]).

Time resolution needs to be improved to observe fast cellular dynamics. Localisation microscopy techniques will benefit from increasing the density of concurrently active probes using multiple-emitter localisation algorithms and localisation strategies based on the statistical analysis of the intensity fluctuations of the fluorophores, such as 3B analysis. It may also involve adopting an improved imaging technology that runs faster than currently available EMCCDs without sacrificing quantum efficiency (possibly based on sCMOS). Photoswitchable probes with fast switching kinetics will be required for live-cell RESOLFT imaging (currently demonstrated on only two). It is noticeable that RESOLFT, LM and SSIM acquisition schemes that are fully compatible with whole live-cell imaging have all been reported in 2012.

Super-resolution will move from cells to tissue and multicellular organisms: Imaging in thick samples is hampered by aberrations and out-of-focus fluorescence. Recent advances that address these problems include precompensation of aberrations through adaptive optics and PSF engineering [57, 64, 214], two-photon activation and/or excitation [58, 59] and the application of light sheet microscopy concepts to PALM [60]. Red-shifted photoconvertible probes will also be demanded for in-depth imaging.

Fluorescence nanoscopy will soon be versatile enough to become available to the wider community as a routine tool. It is not expected that any of the existing strategies will prevail over the others as each working principle offers advantages and disadvantages, and it will be up to the researchers to decide which technique best suits their biological question. Fluorescent nanoscopy has made accessible an entire new level of complexity, particularly in living specimens and its application will keep pushing present instrumental constraints farther.

Acknowledgments The author gratefully acknowledges funding from the Ministerio de Ciencia e Innovación of Spain (MICINN Plan Nacional contract number FIS2009-07966) and the continuing support of the Fundación Biofísica-Bizkaia, in Spain. The author also thanks Gloria de las Heras and Unai Lorenzo for helpful comments and critical revision of the manuscript and Asier Ruiz (Achucarro Basque Centre for Neurosciences) for permission to reproduce Fig. 3.

References

1. Abbe E (1873) Beiträge zur Theorie des Mikroskops und der Mikroskopischen Wahrnehmung. Arch f Mikrosk Anat 9:413–420
2. Hell SW (2003) Toward fluorescence nanoscopy. Nat Biotechnol 21(11):1347–1355

3. Hell SW, Wichmann J (1994) Breaking the diffraction resolution limit by stimulated-emission—stimulated-emission-Depletion fluorescence microscopy. Opt Lett 19(11):780–782
4. Klar TA, Hell SW (1999) Subdiffraction resolution in far-field fluorescence microscopy. Opt Lett 24(14):954–956
5. Klar TA, Jakobs S, Dyba M et al (2000) Fluorescence microscopy with diffraction resolution barrier broken by stimulated emission. Proc Natl Acad Sci U S A 97(15):8206–8210
6. Hell SW, Kroug M (1995) Ground-state-depletion fluorescence microscopy: a concept for breaking the diffraction resolution limit. Appl Phys B Lasers Opt 60(5):495–497
7. Bretschneider S, Eggeling C, Hell SW (2007) Breaking the diffraction barrier in fluorescence microscopy by optical shelving. Phys Rev Lett 98:218103
8. Hofmann M, Eggeling C, Jakobs S et al (2005) Breaking the diffraction barrier in fluorescence microscopy at low light intensities by using reversibly photoswitchable proteins. Proc Natl Acad Sci 102(49):17565–17569
9. Rittweger E, Han KY, Irvine SE et al (2009) STED microscopy reveals crystal colour centres with nanometric resolution. Nat Photon 3(3):144–147
10. Schmidt R, Wurm CA, Jakobs S et al (2008) Spherical nanosized focal spot unravels the interior of cells. Nat Methods 5(6):539–544
11. Willig KI, Harke B, Medda R et al (2007) STED microscopy with continuous wave beams. Nat Methods 4(11). doi:10.1038/nmeth1108
12. Moffitt JR, Osseforth C, Michaelis J (2011) Time-gating improves the spatial resolution of STED microscopy. Opt Express 19(5):4242–4254
13. Vicidomini G, Moneron G, Han KY et al (2011) Sharper low-power STED nanoscopy by time gating. Nat Methods 8(7). doi:10.1038/nmeth.1624
14. Donnert G, Keller J, Wurm CA et al (2007) Two-color far-field fluorescence nanoscopy. Biophys J 92(8):L67–L69
15. Willig KI, Stiel AC, Brakemann T et al (2011) Dual-label STED nanoscopy of living cells using photochromism. Nano Lett 11(9):3970–3973
16. Buckers J, Wildanger D, Vicidomini G et al (2011) Simultaneous multi-lifetime multi-color STED imaging for colocalization analyses. Opt Express 19(4):3130–3143
17. Kastrup L, Blom H, Eggeling C et al (2005) Fluorescence fluctuation spectroscopy in subdiffraction focal volumes. Phys Rev Lett 94(17). doi:10.1103/PhysRevLett.94.178104
18. Eggeling C, Ringemann C, Medda R et al (2009) Direct observation of nanoscale dynamics of membrane lipids in a living cell. Nature 457:1159–1163
19. Ringemann C, Harke B, von Middendorff C et al (2009) Exploring single-molecule dynamics with fluorescence nanoscopy. New J Phys 11. doi:10.1088/1367-2630/11/10/103054
20. Mueller V, Ringemann C, Honigmann A et al (2011) STED nanoscopy reveals molecular details of cholesterol- and cytoskeleton-modulated lipid interactions in living cells. Biophys J 101(7):1651–1660
21. Auksorius E, Boruah BR, Dunsby C et al (2008) Stimulated emission depletion microscopy with a supercontinuum source and fluorescence lifetime imaging. Opt Lett 33(2):113–115
22. Dedecker P, Hotta J, Flors C et al (2007) Subdiffraction imaging through the selective donut-mode depletion of thermally stable photoswitchable fluorophores: numerical analysis and applications to the fluorescent protein Dronpa. J Am Chem Soc 129:16132–16141
23. Grotjohann T, Testa I, Reuss M et al (2012) rsGFP2 enables fast RESOLFT nanoscopy of living cells. eLife 1(e00248). doi:10.7554/eLife.00248
24. Testa I, Urban NT, Jakobs S et al (2012) Nanoscopy of living brain slices with low light levels. Neuron 75(6):992–1000
25. Widengren J, Chmyrov A, Eggeling C et al (2007) Strategies to improve photostabilities in ultrasensitive fluorescence spectroscopy. J Phys Chem A 111(3):429–440
26. Lauterbach MA, Keller J, Schonel A et al (2010) Comparing video-rate STED nanoscopy and confocal microscopy of living neurons. J Biophoton 3(7):417–424
27. Westphal V, Rizzoli SO, Lauterbach MA et al (2008) Video-rate far-field optical nanoscopy dissects synaptic vesicle movement. Science 320(5873):246–249
28. Berning S, Willig KI, Steffens H et al (2012) Nanoscopy in a living mouse brain. Science 335(6068):551–551
29. Pellett PA, Sun XL, Gould TJ et al (2011) Two-color STED microscopy in living cells. Biomed Opt Express 2(8):2364–2371
30. Bingen P, Reuss M, Engelhardt J et al (2011) Parallelized STED fluorescence nanoscopy. Opt Express 19(24):23716–23726
31. Thompson RE, Larson DR, Webb WW (2002) Precise nanometer localization analysis for individual fluorescent probes. Biophys J 82(5):2775–2783
32. Xu K, Babcock HP, Zhuang XW (2012) Dual-objective STORM reveals three-dimensional filament organization in the actin cytoskeleton. Nat Methods 9(2):185–188
33. Aquino D, Schonle A, Geisler C et al (2011) Two-color nanoscopy of three-dimensional volumes by 4Pi detection of stochastically switched fluorophores. Nat Methods 8(4). doi:10.1038/nmeth.1583
34. Betzig E, Patterson GH, Sougrat R et al (2006) Imaging intracellular fluorescent proteins at nanometer resolution. Science 313(5793):1642–1645
35. Rust MJ, Bates M, Zhuang XW (2006) Sub-diffraction-limit imaging by stochastic optical reconstruction microscopy (STORM). Nat Methods 3(10):793–795
36. Hess HF, Girirajan TPK, Mason MD (2006) Ultra-high resolution imaging by fluorescence photoactivation localization microscopy. Biophys J 91:4258–4272
37. Heilemann M, van de Linde S, Mukherjee A et al (2009) Super-resolution imaging with small organic fluorophores. Angew Chem Int Ed 48(37):6903–6908
38. Heilemann M, van de Linde S, Schuttpelz M et al (2008) Subdiffraction-resolution fluorescence imaging with conventional fluorescent probes. Angew Chem Int Ed 47(33):6172–6176
39. Folling J, Bossi M, Bock H et al (2008) Fluorescence nanoscopy by ground-state depletion and single-molecule return. Nat Methods 5(11):943–945
40. Egner A, Geisler C, Von Middendorff C et al (2007) Fluorescence nanoscopy in whole cells by asynchronous localization of photoswitching emitters. Biophys J 93(9):3285–3290
41. Manley S, Gillette JM, Patterson GH et al (2008) High-density mapping of single-molecule trajectories with photoactivated localization microscopy. Nat Methods 5(2):155–157
42. Sharonov A, Hochstrasser RM (2006) Wide-field subdiffraction imaging by accumulated binding of diffusing probes. Proc Natl Acad Sci U S A 103(50):18911–18916
43. Giannone G, Hosy E, Levet F et al (2010) Dynamic superresolution imaging of endogenous proteins on living cells at ultra-high density. Biophys J 99(4):1303–1310
44. Lew MD, Lee SF, Ptacin JL et al (2011) Three-dimensional superresolution colocalization of intracellular protein superstructures and the cell surface in live *Caulobacter crescentus*. Proc Natl Acad Sci U S A 108(46):E1102–E1110
45. Bates M, Huang B, Dempsey GT et al (2007) Multicolor super-resolution imaging with photo-switchable fluorescent probes. Science 317(5845):1749–1753
46. Shroff H, Galbraith CG, Galbraith JA et al (2007) Dual-color superresolution imaging of genetically expressed probes within individual adhesion complexes. Proc Natl Acad Sci U S A 104(51):20308–20313

47. Bossi M, Fölling J, Belov VN et al (2008) Multicolor far-field fluorescence nanoscopy through isolated detection of distinct molecular species. Nanoletters 8(8):2463–2468
48. Andresen M, Stiel AC, Folling J et al (2008) Photoswitchable fluorescent proteins enable monochromatic multilabel imaging and dual color fluorescence nanoscopy. Nat Biotechnol 26(9):1035–1040
49. van de Linde S, Endesfelder U, Mukherjee A et al (2009) Multicolor photoswitching microscopy for subdiffraction-resolution fluorescence imaging. Photochem Photobiol Sci 8(4):465–469
50. Testa I, Wurm CA, Medda R et al (2010) Multicolor fluorescence nanoscopy in fixed and living cells by exciting conventional fluorophores with a single wavelength. Biophys J 99(8):2686–2694
51. Baddeley D, Crossman D, Rossberger S et al (2011) 4D super-resolution microscopy with conventional fluorophores and single wavelength excitation in optically thick cells and tissues. PLoS One 6(5):e20645. doi:10.1371/journal.pone.0020645
52. Bates M, Dempsey GT, Chen KH et al (2012) Multicolor super-resolution fluorescence imaging via multi-parameter fluorophore detection. Chemphyschem 13(1):99–107
53. Juette MF, Gould TJ, Lessard MD et al (2008) Three-dimensional sub-100 nm resolution fluorescence microscopy of thick samples. Nat Methods 5(6):527–529
54. Huang B, Wang W, Bates M et al (2008) Three-dimensional super-resolution imaging by stochastic optical reconstruction microscopy. Science 319:810–813
55. Pavani SRP, Thompson MA, Biteen JS et al (2009) Three-dimensional, single-molecule fluorescence imaging beyond the diffraction limit by using a double-helix point spread function. Proc Natl Acad Sci U S A 106(9):2995–2999
56. Baddeley D, Cannell M, Soeller C (2011) Three-dimensional sub-100 nm super-resolution imaging of biological samples using a phase ramp in the objective pupil. Nano Res 4(6):589–598
57. Izeddin I, El Beheiry M, Andilla J et al (2012) PSF shaping using adaptive optics for three-dimensional single-molecule super-resolution imaging and tracking. Opt Express 20(5):4957–4967
58. Vaziri A, Tang JY, Shroff H et al (2008) Multilayer three-dimensional super resolution imaging of thick biological samples. Proc Natl Acad Sci U S A 105(51):20221–20226
59. York AG, Ghitani A, Vaziri A et al (2011) Confined activation and subdiffractive localization enables whole-cell PALM with genetically expressed probes. Nat Methods 8(4). doi:10.1038/nmeth.1571
60. Zanacchi FC, Lavagnino Z, Perrone Donnorso M et al (2011) Live-cell 3D superresolution imaging in thick biological samples. Nat Methods 8:1047–1049
61. Shtengel G, Galbraith JA, Galbraith CG et al (2009) Interferometric fluorescent super-resolution microscopy resolves 3D cellular ultrastructure. Proc Natl Acad Sci U S A 106(9):3125–3130
62. Tokunaga M, Imamoto N, Sakata-Sogawa K (2008) Highly inclined thin illumination enables clear single-molecule imaging in cells. Nat Methods 5(2):159–161
63. Badieirostami M, Lew MD, Thompson MA et al (2010) Three-dimensional localization precision of the double-helix point spread function versus astigmatism and biplane. Appl Phys Lett 97(16):161103. doi:10.1063/1.3499652
64. Quirin S, Pavani SRP, Piestun R (2012) Optimal 3D single-molecule localization for superresolution microscopy with aberrations and engineered point spread functions. Proc Natl Acad Sci U S A 109(3):675–679
65. Huisken J, Swoger J, Del Bene F et al (2004) Optical sectioning deep inside live embryos by selective plane illumination microscopy. Science 305(5686):1007–1009
66. Andersson SB (2008) Localization of a fluorescent source without numerical fitting. Opt Express 16(23):18714–18724
67. Parthasarathy R (2012) Rapid, accurate particle tracking by calculation of radial symmetry centers. Nat Methods 9(7). doi:10.1038/nmeth.2071
68. Ma HQ, Long F, Zeng SQ et al (2012) Fast and precise algorithm based on maximum radial symmetry for single molecule localization. Opt Lett 37(13):2481–2483
69. Hedde PN, Fuchs J, Oswald F et al (2009) Online image analysis software for photoactivation localization microscopy. Nat Methods 6(10):689–690
70. Wolter S, Loschberger A, Holm T et al (2012) rapidSTORM: accurate, fast open-source software for localization microscopy. Nat Methods 9(11):1040–1041
71. Henriques R, Lelek M, Fornasiero EF et al (2010) QuickPALM: 3D real-time photoactivation nanoscopy image processing in image. J Nat Methods 7(5):339–340
72. Mortensen KI, Churchman LS, Spudich JA et al (2010) Optimized localization analysis for single-molecule tracking and super-resolution microscopy. Nat Methods 7(5). doi:10.1038/nmeth.1447
73. Smith CS, Joseph N, Rieger B et al (2010) Fast, single-molecule localization that achieves theoretically minimum uncertainty. Nat Methods 7(5). doi:10.1038/nmeth.1449
74. Quan TW, Li PC, Long F et al (2010) Ultra-fast, high-precision image analysis for localization-based super resolution microscopy. Opt Express 18(11):11867–11876
75. Stallinga S, Rieger B (2010) Accuracy of the Gaussian point spread function model in 2D localization microscopy. Opt Express 18(24):24461–24476
76. Engelhardt J, Keller J, Hoyer P et al (2011) Molecular orientation affects localization accuracy in superresolution far-field fluorescence microscopy. Nano Lett 11(1):209–213
77. Backlund MP, Lew MD, Backer AS et al (2012) Simultaneous, accurate measurement of the 3D position and orientation of single molecules. Proc Natl Acad Sci U S A 109(47):19087–19092
78. Stallinga S, Rieger B (2012) Position and orientation estimation of fixed dipole emitters using an effective Hermite point spread function model. Opt Express 20(6):5896–5921
79. Mlodzianoski MJ, Schreiner JM, Callahan SP et al (2011) Sample drift correction in 3D fluorescence photoactivation localization microscopy. Opt Express 19(16):15009–15019
80. Geisler C, Hotz T, Schonle A et al (2012) Drift estimation for single marker switching based imaging schemes. Opt Express 20(7):7274–7289
81. Flors C, Hotta J, Uji-I H et al (2007) A stroboscopic approach for fast photoactivation-localization microscopy with Dronpa mutants. J Am Chem Soc 129(45):13970–13977
82. Jones SA, Shim SH, He J et al (2011) Fast, three-dimensional super-resolution imaging of live cells. Nat Methods 8(6). doi:10.1038/nmeth.1605
83. Shroff H, Galbraith CG, Galbratih JA et al (2008) Live-cell photoactivated localization microscopy of nanoscale adhesion dynamics. Nat Methods 5(5):417–423
84. Wolter S, Endesfelder U, van de Linde S et al (2011) Measuring localization performance of super-resolution algorithms on very active samples. Opt Express 19(8):7020–7033
85. Frost NA, Shroff H, Kong HH et al (2010) Single-molecule discrimination of discrete perisynaptic and distributed sites of actin filament assembly within dendritic spines. Neuron 67(1):86–99
86. Holden SJ, Uphoff S, Kapanidis AN (2011) DAOSTORM: an algorithm for high-density super-resolution microscopy. Nat Methods 8(4):279–280
87. Huang F, Schwartz SL, Byars JM et al (2011) Simultaneous multiple-emitter fitting for single molecule super-resolution imaging. Biomed Opt Express 2(5):1377–1393
88. Zhu L, Zhang W, Elnatan D et al (2012) Faster STORM using compressed sensing. Nat Methods 9(7). doi:10.1038/nmeth.1978

89. Dedecker P, Mo GCH, Dertinger T et al (2012) Widely accessible method for superresolution fluorescence imaging of living systems. Proc Natl Acad Sci U S A 109(27):10909–10914
90. Dertinger T, Colyer R, Iyer G et al (2009) Fast, background-free, 3D super-resolution optical fluctuation imaging (SOFI). Proc Natl Acad Sci U S A 106(52):22287–22292
91. Quan TW, Zhu HY, Liu XM et al (2011) High-density localization of active molecules using structured sparse model and Bayesian information criterion. Opt Express 19(18):16963–16974
92. Cox S, Rosten E, Monypenny J et al (2012) Bayesian localization microscopy reveals nanoscale podosome dynamics. Nat Methods 9(2). doi:10.1038/nmeth.1812
93. Maji S, Bruchez MP (2012) Inferring biological structures from super-resolution single molecule images using generative models. Plos One 7(5). doi:10.1371/journal.pone.0036973
94. Burnette DT, Sengupta P, Dai YH et al (2011) Bleaching/blinking assisted localization microscopy for superresolution imaging using standard fluorescent molecules. Proc Natl Acad Sci U S A 108(52):21081–21086
95. Hu YS, Nan X, Sengupta P et al (2013) Accelerating 3B single-molecule super-resolution microscopy with cloud computing. Nat Methods 10(2):96–97
96. Baddeley D, Cannell MB, Soeller C (2010) Visualization of localization microscopy data. Microsc Microanal 16(1):64–72
97. Krizek P, Raska I, Hagen GM (2011) Minimizing detection errors in single molecule localization microscopy. Opt Express 19(4):3226–3235
98. Neil MAA, Juskaitis R, Wilson T (1997) Method of obtaining optical sectioning by using structured light in a conventional microscope. Opt Lett 22(24):1905–1907
99. Gustafsson MGL (2000) Surpassing the lateral resolution limit by a factor of two using structured illumination microscopy. J Microsc-Oxf 198(2):82–87
100. Schermelleh L, Carlton PM, Haase S et al (2008) Subdiffraction multicolor imaging of the nuclear periphery with 3D structured illumination microscopy. Science 320(5881):1332–1336
101. Heintzmann R, Jovin TM, Cremer C (2002) Saturated patterned excitation microscopy—a concept for optical resolution improvement. J Opt Soc Am A 19(8):1599–1609
102. Gustafsson MGL (2005) Nonlinear structured-illumination microscopy: wide-field fluorescence imaging with theoretically unlimited resolution. Proc Natl Acad Sci 102(37):13081–13086
103. Rego EH, Shao L, Macklin JJ et al (2012) Nonlinear structured-illumination microscopy with a photoswitchable protein reveals cellular structures at 50-nm resolution. Proc Natl Acad Sci U S A 109(3):E135–E143
104. Gustafsson MGL, Shao L, Carlton PM et al (2008) Three-dimensional resolution doubling in wide-field fluorescence microscopy by structured illumination. Biophys J 94(12):4957–4970
105. Shao L, Kner P, Hesper Rego E et al (2011) Super-resolution 3D microscopy of live whole cells using structured illumination. Nat Methods 8(12):1044–1046
106. York AG, Parekh SH, Nogare DD et al (2012) Resolution doubling in live, multicellular organisms via multifocal structured illumination microscopy. Nat Methods 9(7). doi:10.1038/nmeth.2025
107. Kuang CF, Zhao W, Wang GR (2010) Far-field optical nanoscopy based on continuous wave laser stimulated emission depletion. Rev Sci Instrum 81(5):053709. doi:10.1063/1.3432001
108. Wildanger D, Rittweger E, Kastrup L et al (2008) STED microscopy with a supercontinuum laser source. Opt Express 16(13):9614–9621
109. Donnert G, Keller J, Medda R et al (2006) Macromolecular-scale resolution in biological fluorescence microscopy. Proc Natl Acad Sci U S A 103(31):11440–11445
110. Sieber JJ, Willig KI, Heintzmann R et al (2006) The SNARE motif is essential for the formation of syntaxin clusters in the plasma membrane. Biophys J 90:2843–2851
111. Willig KI, Keller J, Bossi M et al (2006) STED microscopy resolves nanoparticles assemblies. New J Phys 8. doi:10.1088/1367-2630/8/6/106
112. Willig KI, Kellner RR, Medda R et al (2006) Nanoscale resolution in GFP-based microscopy. Nat Methods 3(9):721–723
113. Nagerl UV, Willig KI, Hein B et al (2008) Live-cell imaging of dendritic spines by STED microscopy. Proc Natl Acad Sci U S A 105(48):18982–18987
114. Hein B, Willig KI, Hell SW (2008) Stimulated emission depletion (STED) nanoscopy of a fluorescent protein-labeled organelle inside a living cell. Proc Natl Acad Sci 105(38):14271–14276
115. Morozova KS, Piatkevich KD, Gould TJ et al (2010) Far-red fluorescent protein excitable with red lasers for flow cytometry and superresolution STED nanoscopy. Biophys J 99(2):L13–L15
116. Strack RL, Hein B, Bhattacharyya D et al (2009) A rapidly maturing far-red derivative of DsRed-Expres2 for whole-cell labeling. Biochemistry 48(35):8279–8281
117. Brakemann T, Stiel AC, Weber G et al (2011) A reversibly photoswitchable GFP-like protein with fluorescence excitation decoupled from switching. Nat Biotechnol 29(10). doi:10.1038/nbt.1952
118. Los GV, Encell LP, McDougall MG et al (2008) HatoTag: a novel protein labeling technology for cell imaging and protein analysis. ACS Chem Biol 3(6):373–382
119. Schroder J, Benink H, Dyba M et al (2009) In vivo labeling method using a genetic construct for nanoscale resolution microscopy. Biophys J 96(1):L1–L3
120. Keppler A, Gendreizig S, Gronemeyer T et al (2003) A general method for the covalent labeling of fusion proteins with small molecules in vivo. Nat Biotechnol 21(1):86–89
121. Gautier A, Juillerat A, Heinis C et al (2008) An engineered protein tag for multiprotein labeling in living cells. Chem Biol 15(2):128–136
122. Hein B, Willig KI, Wurm CA et al (2010) Stimulated emission depletion nanoscopy of living cells using SNAP-Tag fusion proteins. Biophys J 98(1):158–163
123. Ormo M, Cubitt AB, Kallio K et al (1996) Crystal structure of the *Aequorea victoria* green fluorescent protein. Science 273(5280):1392–1395
124. Wombacher R, Heidbreder M, van de Linde S et al (2010) Live-cell super-resolution imaging with trimethoprim conjugates. Nat Methods 7(9):717–719
125. Klein T, Loschberger A, Proppert S et al (2011) Live-cell dSTORM with SNAP-tag fusion proteins. Nat Methods 8(1):7–9
126. Patterson GH, Lippincott-Schwartz J (2002) A photoactivatable GFP for selective photolabeling of proteins and cells. Science 297(5588):1873–1877
127. Subach FV, Patterson GH, Manley S et al (2009) Photoactivatable mCherry for high-resolution two-color fluorescence microscopy. Nat Methods 6(2):153–159
128. Gunewardene MS, Subach FV, Gould TJ et al (2011) Superresolution imaging of multiple fluorescent proteins with highly overlapping emission spectra in living cells. Biophys J 101(6):1522–1528
129. Verkhusha VV, Sorkin A (2005) Conversion of the monomeric red fluorescent protein into a photoactivatable probe. Chem Biol 12(3):279–285
130. Subach FV, Patterson GH, Renz M et al (2010) Bright monomeric photoactivatable red fluorescent protein for two-color super-resolution sptPALM of live cells. J Am Chem Soc 132(18):6481–6491
131. Gurskaya NG, Verkhusha VV, Shcheglov AS et al (2006) Engineering of a monomeric green-to-red photoactivatable fluorescent protein induced by blue light. Nat Biotechnol 24(4):461–465
132. Hoi HF, Shaner NC, Davidson MW et al (2010) A monomeric photoconvertible fluorescent protein for imaging of dynamic protein localization. J Mol Biol 401(5):776–791

133. McKinney SA, Murphy CS, Hazelwood KL et al (2009) A bright and photostable photoconvertible fluorescent protein. Nat Methods 6(2):131–133
134. Zhang MS, Chang H, Zhang YD et al (2012) Rational design of true monomeric and bright photoactivatable fluorescent proteins. Nat Methods 9(7). doi:10.1038/nmeth.2021
135. Habuchi S, Tsutsui H, Kochaniak AB et al (2008) mKikGR, a monomeric photoswitchable fluorescent protein. PLoS One 3(12):e3944. doi:10.1371/journal.pone.0003944
136. McEvoy AL, Hoi H, Bates M et al (2012) mMaple: a photoconvertible fluorescent protein for use in multiple imaging modalities. PLoS One 7(12):e51314. doi:10.1371/journal.pone.0051314
137. Chudakov DM, Verkhusha VV, Staroverov DB et al (2004) Photoswitchable cyan fluorescent protein for protein tracking. Nat Biotechnol 22(11):1435–1439
138. Subach OM, Patterson GH, Ting LM et al (2011) A photoswitchable orange-to-far-red fluorescent protein, PSmOrange. Nat Methods 8(9). doi:10.1038/nmeth.1664
139. Ando R, Mizuno H, Miyawaki A (2004) Regulated fast nucleocytoplasmic shuttling observed by reversible protein highlighting. Science 306(5700):1370–1373
140. Chang H, Zhang MS, Ji W et al (2012) A unique series of reversibly switchable fluorescent proteins with beneficial properties for various applications. Proc Natl Acad Sci U S A 109(12):4455–4460
141. Stiel AC, Andresen M, Bock H et al (2008) Generation of monomeric reversibly switchable red fluorescent proteins for far-field fluorescence nanoscopy. Biophys J 95:2989–2997
142. Stiel AC, Trowitzsch S, Weber G et al (2007) 1.8 angstrom bright-state structure of the reversibly switchable fluorescent protein Dronpa guides the generation of fast switching variants. Biochem J 402:35–42
143. van Thor JJ, Gensch T, Hellingwerf KJ et al (2002) Phototransformation of green fluorescent protein with UV and visible light leads to decarboxylation of glutamate 222. Nat Struct Biol 9(1):37–41
144. Wiedenmann J, Ivanchenko S, Oswald F et al (2004) EosFP, a fluorescent marker protein with UV-inducible green-to-red fluorescence conversion. Proc Natl Acad Sci U S A 101(45):15905–15910
145. Habuchi S, Ando R, Dedecker P et al (2005) Reversible single-molecule photoswitching in the GFP-like fluorescent protein Dronpa. Proc Natl Acad Sci U S A 102(27):9511–9516
146. Habuchi S, Dedecker P, Hotta JI et al (2006) Photo-induced protonation/deprotonation in the GFP-like fluorescent protein Dronpa: mechanism responsible for the reversible photoswitching. Photochem Photobiol Sci 5(6):567–576
147. Andresen M, Stiel AC, Trowitzsch S et al (2007) Structural basis for reversible photoswitching in Dronpa. Proc Natl Acad Sci U S A 104(32):13005–13009
148. Heilemann M, Margeat E, Kasper R et al (2005) Carbocyanine dyes as efficient reversible single-molecule optical switch. J Am Chem Soc 127(11):3801–3806
149. Vogelsang J, Cordes T, Forthmann C et al (2009) Controlling the fluorescence of ordinary oxazine dyes for single-molecule switching and superresolution microscopy. Proc Natl Acad Sci U S A 106(20):8107–8112
150. Dempsey GT, Vaughan JC, Chen KH et al (2011) Evaluation of fluorophores for optimal performance in localization-based super-resolution imaging. Nat Meth 8(12):1027–1036
151. Lee HLD, Lord SJ, Iwanaga S et al (2010) Superresolution imaging of targeted proteins in fixed and living cells using photoactivatable organic fluorophores. J Am Chem Soc 132(43):15099–15101
152. Griffin BA, Adams SR, Tsien RY (1998) Specific covalent labeling of recombinant protein molecules inside live cells. Science 281(5374):269–272
153. Lelek M, Di Nunzio F, Henriques R et al (2012) Superresolution imaging of HIV in infected cells with FlAsH-PALM. Proc Natl Acad Sci U S A 109(22):8564–8569
154. Wilmes S, Staufenbiel M, Lisse D et al (2012) Triple-color super-resolution imaging of live cells: resolving submicroscopic receptor organization in the plasma membrane. Angew Chem-Int Ed 51(20):4868–4871
155. Shannon CE (1949) Communication in the presence of noise. Proc Inst Radio Eng 37(1):10–21
156. Ram S, Ward ES, Ober RJ (2006) Beyond Rayleigh's criterion: a resolution measure with application to single-molecule microscopy. Proc Natl Acad Sci U S A 103(12):4457–4462
157. Fitzgerald JE, Lu J and Schnitzer MJ (2012) Estimation theoretic measure of resolution for stochastic localization microscopy. Phys Rev Lett 109(4):048102
158. Mukamel EA, Schnitzer MJ (2012) Unified resolution bounds for conventional and stochastic localization fluorescence microscopy. Phys Rev Lett 109(16):168102
159. Ripley BD (1977) Modeling spatial patterns. J R Stat Soc Ser B Methodol 39(2):172–212
160. Kiskowski MA, Hancock JF, Kenworthy AK (2009) On the use of Ripley's K-function and its derivatives to analyze domain size. Biophys J 97:1095–1103
161. Annibale P, Vanni S, Scarselli M et al (2011) Quantitative photo activated localization microscopy: unraveling the effects of photoblinking. PLoS One 6(7):e22678. doi:10.1371/journal.pone.0022678
162. Annibale P, Vanni S, Scarselli M et al (2011) Identification of clustering artifacts in photoactivated localization microscopy. Nat Methods 8(7):527–528
163. Veatch SL, Machta BB, Shelby SA et al (2012) Correlation functions quantify super-resolution images and estimate apparent clustering due to over-counting. PLoS One 7(2):e31457. doi:10.1371/journal.pone.0031457
164. Sengupta P, Lippincott-Schwartz J (2012) Quantitative analysis of photoactivated localization microscopy (PALM) datasets using pair-correlation analysis. Bioessays 34(5):396–405
165. Sengupta P, Jovanovic-Talisman T, Lippincott-Schwartz J (2013) Quantifying spatial organization in point-localization superresolution images using pair correlation analysis. Nat Protoc 8(2):345–354
166. Sengupta P, Jovanovic-Talisman T, Skoko D et al (2011) Probing protein heterogeneity in the plasma membrane using PALM and pair correlation analysis. Nat Meth 8(11):969–975
167. Watanabe S, Punge A, Hollopeter G et al (2011) Protein localization in electron micrographs using fluorescence nanoscopy. Nat Methods 8(1). doi:10.1038/nmeth.1537
168. Kopek BG, Shtengel G, Xu CS et al (2012) Correlative 3D superresolution fluorescence and electron microscopy reveal the relationship of mitochondrial nucleoids to membranes. Proc Natl Acad Sci U S A 109(16):6136–6141
169. Sharma S, Santiskulvong C, Bentolila LA et al (2012) Correlative nanomechanical profiling with super-resolution F-actin imaging reveals novel insights into mechanisms of cisplatin resistance in ovarian cancer cells. Nanomed Nanotechnol Biol Med 8(5):757–766
170. Kanchanawong P, Shtengel G, Pasapera AM et al (2010) Nanoscale architecture of integrin-based cell adhesions. Nature 468(7323). doi:10.1038/nature09621
171. Rossier O, Octeau V, Sibarita JB et al (2012) Integrins beta(1) and beta(3) exhibit distinct dynamic nanoscale organizations inside focal adhesions. Nat Cell Biol 14(10). doi:10.1038/ncb2588
172. Shim SH, Xia CL, Zhong GS et al (2012) Super-resolution fluorescence imaging of organelles in live cells with photoswitchable membrane probes. Proc Natl Acad Sci U S A 109(35):13978–13983
173. Lakadamyali M, Babcock H, Bates M et al (2012) 3D multicolor super-resolution imaging offers improved accuracy in neuron tracing. PLoS One 7(1):e30826. doi:10.1371/journal.pone.0030826
174. van de Linde S, Sauer M, Heilemann M (2008) Subdiffraction-resolution fluorescence imaging of proteins in the mitochondrial

inner membrane with photoswitchable fluorophores. J Struct Biol 164(3):250–254
175. Wurm CA, Neumann D, Lauterbach MA et al (2011) Nanoscale distribution of mitochondrial import receptor Tom20 is adjusted to cellular conditions and exhibits an inner-cellular gradient. Proc Natl Acad Sci U S A 108(33):13546–13551
176. Appelhans T, Richter CP, Wilkens V et al (2012) Nanoscale organization of mitochondrial microcompartments revealed by combining tracking and localization microscopy. Nano Lett 12(2):610–616
177. Loschberger A, van de Linde S, Dabauvalle MC et al (2012) Super-resolution imaging visualizes the eightfold symmetry of gp210 proteins around the nuclear pore complex and resolves the central channel with nanometer resolution. J Cell Sci 125(3):570–575
178. Yao J, Fetter RD, Hu P et al (2011) Subnuclear segregation of genes and core promoter factors in myogenesis. Genes Dev 25(6):569–580
179. Bohn M, Diesinger P, Kaufmann R et al (2010) Localization microscopy reveals expression-dependent parameters of chromatin nanostructure. Biophys J 99(5):1358–1367
180. Flors C, Ravarani CNJ, Dryden DTF (2009) Super-resolution imaging of DNA labelled with intercalating dyes. Chemphyschem 10(13):2201–2204
181. Flors C (2010) Photoswitching of monomeric and dimeric DNA-intercalating cyanine dyes for super-resolution microscopy applications. Photochem Photobiol Sci 9(5):643–648
182. Flors C (2011) DNA and chromatin imaging with super-resolution fluorescence microscopy based on single-molecule localization. Biopolymers 95(5):290–297
183. Zessin PJM, Finan K, Heilemann M (2012) Super-resolution fluorescence imaging of chromosomal DNA. J Struct Biol 177(2):344–348
184. Lee SF, Thompson MA, Schwartz MA et al (2011) Super-resolution imaging of the nucleoid-associated protein HU in *Caulobacter crescentus*. Biophys J 100(7):L31–L33
185. Wang WQ, Li GW, Chen CY et al (2011) Chromosome organization by a nucleoid-associated protein in live bacteria. Science 333(6048):1445–1449
186. Owen DM, Rentero C, Rossy J et al (2010) PALM imaging and cluster analysis of protein heterogeneity at the cell surface. J Biophoton 3(7):446–454
187. Kellner RR, Baier CJ, Willig KI et al (2007) Nanoscale organization of nicotinic acetylcholine receptors revealed by stimulated emission depletion microscopy. Neuroscience 144(1):135–143
188. Hess ST, Gould TJ, Gudheti MV et al (2007) Dynamic clustered distribution of hemagglutinin resolved at 40 nm in living cell membranes discriminates between raft theories. Proc Natl Acad Sci U S A 104(44):17370–17375
189. Scarselli M, Annibale P, Radenovic A (2012) Cell type-specific beta 2-adrenergic receptor clusters identified using photoactivated localization microscopy are not lipid raft related, but depend on actin cytoskeleton integrity. J Biol Chem 287(20):16768–16780
190. Mizuno H, Abe M, Dedecker P et al (2011) Fluorescent probes for superresolution imaging of lipid domains on the plasma membrane. Chem Sci 2(8):1548–1553
191. Kuo CK, Hochstrasser RM (2011) Super-resolution microscopy of lipid bilayer phases. J Am Chem Soc 133(13):4664–4667
192. Sieber JJ, Willig KI, Kutzner C et al (2007) Anatomy and dynamics of a supramolecular membrane protein cluster. Science 317(5841):1072–1076
193. van den Bogaart G, Meyenberg K, Risselada HJ et al (2011) Membrane protein sequestering by ionic protein–lipid interactions. Nature 479(7374):552–555
194. Bar-On D, Wolter S, van de Linde S et al (2012) Super-resolution imaging reveals the internal architecture of nano-sized syntaxin clusters. J Biol Chem 287(32):27158–27167
195. Hsu CJ, Baumgart T (2011) Spatial association of signaling proteins and F-actin effects on cluster assembly analyzed via photoactivation localization microscopy in T cells. PLoS One 6(8):e23586. doi:10.1371/journal.pone.0023586
196. Lillemeier BF, Mortelmaier MA, Forstner MB et al (2010) TCR and Lat are expressed on separate protein islands on T cell membranes and concatenate during activation. Nat Immunol 11(1). doi:10.1038/ni.1832
197. Williamson DJ, Owen DM, Rossy J et al (2011) Pre-existing clusters of the adaptor Lat do not participate in early T cell signaling events. Nat Immunol 12(7). doi:10.1038/ni.2049
198. Brown ACN, Oddos S, Dobbie IM et al (2011) Remodelling of cortical actin where lytic granules dock at natural killer cell immune synapses revealed by super-resolution microscopy. Plos Biol 9(9):e1001152. doi:10.1371/journal.pbio.1001152
199. Opazo F, Punge A, Bueckers J et al (2010) Limited intermixing of synaptic vesicle components upon vesicle recycling. Traffic 11(6):800–812
200. Willig KI, Rizzoli SO, Westphal V et al (2006) STED microscopy reveals that synaptotagmin remains clustered after synaptic vesicle exocytosis. Nature 440(7086):935–939
201. Hoopmann P, Punge A, Barysch SV et al (2010) Endosomal sorting of readily releasable synaptic vesicles. Proc Natl Acad Sci U S A 107(44):19055–19060
202. Dean C, Liu H, Staudt T et al (2012) Distinct subsets of Syt-IV/BDNF vesicles are sorted to axons versus dendrites and recruited to synapses by activity. J Neurosci 32(16):5398–5413
203. Kamin D, Lauterbach MA, Westphal V et al (2010) High- and low-mobility stages in the synaptic vesicle cycle. Biophys J 99(2):675–684
204. Hoze N, Nair D, Hosy E et al (2012) Heterogeneity of AMPA receptor trafficking and molecular interactions revealed by superresolution analysis of live cell imaging. Proc Natl Acad Sci U S A 109(42):17052–17057
205. Izeddin I, Specht CG, Lelek M et al (2011) Super-resolution dynamic imaging of dendritic spines using a low-affinity photoconvertible actin probe. PLoS One 6(1):e15611. doi:10.1371/journal.pone.0015611
206. Dani A, Huang B, Bergan J et al (2010) Superresolution imaging of chemical synapses in the brain. Neuron 68(5):843–856
207. Riedl J, Crevenna AH, Kessenbrock K et al (2008) Lifeact: a versatile marker to visualize F-actin. Nat Methods 5(7):605–607
208. Urban NT, Willig KI, Hell SW et al (2011) STED nanoscopy of actin dynamics in synapses deep inside living brain slices. Biophys J 101(5):1277–1284
209. Gunzenhauser J, Olivier N, Pengo T et al (2012) Quantitative super-resolution imaging reveals protein stoichiometry and nanoscale morphology of assembling HIV-Gag virions. Nano Lett 12(9):4705–4710
210. Lehmann M, Rocha S, Mangeat B et al (2011) Quantitative multicolor super-resolution microscopy reveals tetherin HIV-1 interaction. PLoS Pathog 7(12):e1002456. doi:10.1371/journal.ppat.1002456
211. Malkusch S, Muranyi W, Muller B et al (2013) Single-molecule coordinate-based analysis of the morphology of HIV-1 assembly sites with near-molecular spatial resolution. Histochem Cell Biol 139(1):173–179
212. Chojnacki J, Staudt T, Glass B et al (2012) Maturation-dependent HIV-1 surface protein redistribution revealed by fluorescence nanoscopy. Science 338(6106):524–528
213. Ries J, Kaplan C, Platonova E et al (2012) A simple, versatile method for GFP-based super-resolution microscopy via nanobodies. Nat Methods 9(6). doi:10.1038/nmeth.1991
214. Gould TJ, Burke D, Bewersdorf J et al (2012) Adaptive optics enables 3D STED microscopy in aberrating specimens. Opt Express 20(19):20998–21009